Snip1–PRC2 governs the intrinsic apoptosis program in the developing brain

Yurika Matsui[1], Mohamed Nadhir Djekidel[2], Katherine Lindsay[1], Parimal Samir[1,3], Nina Connolly[1], Hongfeng Chen[1], Yiping Fan[2], Beisi Xu[2], Jamy C. Peng[1,*]

[1]Department of Developmental Neurobiology, [2]Center for Applied Bioinformatics, St. Jude Children's Research Hospital, 262 Danny Thomas Place, Memphis, TN 38105 USA

[3]Present address: Department of Microbiology and Immunology, University of Texas Medical Branch, 301 University Blvd, Medical Research Building, Room 7, 138E, Galveston, TX 77550 USA

*Corresponding author: Jamy C. Peng jamy.peng@stjude.org

Running Title:
PRC2–Snip1 interaction controls apoptosis

ABSTRACT

Brain development requires the intricate balance between division, death, and differentiation of neural progenitor cells (NPCs). Here, we report the discovery of Snip1 as a key regulator of NPC self-renewal and death. In the embryonic brain, Snip1 depletion causes brain dysplasia with robust induction of apoptosis. In culture, Snip1-depleted NPCs had reduced self-renewing property. Snip1 protein binds to promoters and regulates the expression of genes involved in intrinsic apoptosis, cell division, and cortical development. The depletion of a key chromatin modifier Polycomb Repressive Complex 2 (PRC2) is sufficient to reduce apoptosis and partially rescue the development of the Snip1-depleted brain. PRC2 controls NPC expansion, brain regionalization, and cell fate specification by depositing H3K27me3 and suppressing transcription by RNA polymerase II. Our findings suggest that Snip1 exerts loci-dependent regulation of PRC2 and H3K27me3 to toggle between death, survival, and self-renewal in the developing brain.

INTRODUCTION

Neural progenitor cells (NPCs) are self-renewing and multipotent cells that give rise to neurons, oligodendrocytes, and astrocytes in the central nervous system (CNS). The appropriate size and structural organization of the brain is achieved by the exquisite balance between division, death, and differentiation of NPCs. Cell death is prominent particularly in the normal developing brain, most of which is observed in the proliferative zones of the cortex where NPCs reside (Bieberich et al., 2001; Blaschke et al., 1996; Sommer and Rao, 2002; Thomaidou et al., 1997). However, how NPCs are developmentally programmed to toggle between survival and death is poorly understood.

The cell-intrinsic control of NPCs is mediated through epigenetic mechanisms, and a key epigenetic modifier is Polycomb repressive complex 2 (PRC2). PRC2 deposits H3K27 trimethylation (H3K27me3), mediates chromatin compaction, and suppresses RNA polymerase II–dependent transcription (Chang et al., 2021; Holoch and Margueron, 2017; Laugesen et al., 2019; Pasini et al., 2004; von Schimmelmann et al., 2016). Genetic deletions of PRC2 subunits cause embryonic lethality with gastrulation failure (Faust et al., 1998; Faust et al., 1995; O'Carroll et al., 2001; Pasini et al., 2004). PRC2 is essential for CNS development, including neural tube closure, expansion of NPCs, and neuronal versus glial fate specification (Pasini et al., 2007; Pereira et al., 2010; Takeuchi et al., 1995). In addition, fine-tuning H3K27me3 deposition in the brain has been found critical for maintaining the viability of neural cells (Chang et al., 2021; Li et al., 2013; von Schimmelmann et al., 2016). Studies in mouse models have shown that aberrant increases of H3K27me3 are observed in ataxia-telangiectasia, whereas H3K27me3 reduction is linked to neural loss in ischemic brain injuries or Huntington's disease (Chang et al., 2021; Li et al., 2013; von Schimmelmann et al., 2016). Here, we report physical and functional interactions between PRC2 and Smad nuclear interacting protein 1 (Snip1) in controlling survival and death of NPCs.

Snip1 was originally discovered by a yeast two-hybrid screen for interactors of SMAD proteins (Kim et al., 2000). The N-terminus of SNIP1 binds to histone acetyltransferases p300/CBP at their CH1 domain to disrupt the SMAD4–p300/CBP complex formation and dampen BMP/TGFβ signaling (Feng et al., 1998; Janknecht et al., 1998; Pouponnot et al., 1998; Topper et al., 1998). SNIP1 can also dampen NFκB signaling by disrupting RELA/p65-p300/CBP complex formation (Gerritsen et al., 1997; Kim et al., 2001; Perkins et al., 1997; Vanden Berghe et al., 1999; Zhong et al., 1998). Besides its role as a transcriptional suppressor to dampen TGFβ or NFκB signaling, SNIP1 can recruit c-MYC to p300/CBP and enhance c-MYC–mediated cell transformation (Fujii et al., 2006). Ectopic expression of Snip1 induces defective patterning in *Xenopus* embryos (Kim et al., 2000). Global knockout (KO) of Snip1 in zebrafish embryos causes microcephaly with reduction in GABAergic and glutamatergic neurons (Fernandez et al., 2018).

Here, we report that Snip1 is required for the survival and self-renewal of NPCs in the embryonic brain. Using conditional KO to deplete Snip1 in NPCs, we revealed that Snip1 modulates gene expression programs to suppress intrinsic apoptosis and safeguard proper cell division and cortical development. Mechanistically, we uncovered that Snip1 physically binds to PRC2 and occupies PRC2 targets on chromatin for gene regulation. The KO of a PRC2 subunit Eed reduces apoptosis and alleviates brain dysplasia in Snip1-KO embryos, thus revealing the crucial genetic interaction of Snip1-PRC2 for gatekeeping the multiple critical properties of NPCs *in vivo*.

RESULTS

Snip1 is required for the survival of NPCs in the murine embryonic brain

We examined the expression of Snip1 in the murine embryonic brain by RNAscope (Wang et al., 2012). At embryonic day E11.5 and E13.5, *Snip1* transcripts were expressed in nearly all cells and robustly expressed in the neuroepithelia lining the ventricles, where NPCs reside (Supp Fig 1a-b). To study Snip1 in the murine embryonic brain, we used *Nestin* (*Nes*)::*Cre* to conditionally deplete Snip1 in NPCs, hereafter referred to as *Snip1*^{Nes}-KO. *Nes*::Cre is expressed in NPCs to recombine flox sites and excise exon 2 of *Snip1* (Fig 1a, Supp Fig 1c-d, Supp Fig 2). *Snip1*^{Nes}*-KO* embryos displayed severe thinning of brain tissues and dysplasia with 100% penetrance (Fig 1b-c, $p<0.0001$ by Fisher's exact test). To examine the cellular underpinnings of the brain dysplasia in *Snip1*^{Nes}-KO, we looked at levels of cell proliferation and apoptosis. Mouse NPCs were identified by their expression of the neural stem cell marker Sox2. To identify proliferating cells in vivo, we injected BrdU into pregnant dams and/or detected the proliferative marker Ki67. Quantification of these markers in neuroepithelia did not reveal significant difference in proliferative NPCs in sibling control and *Snip1*^{Nes}-KO embryos (Supp Fig 3).

We next examined apoptosis by IF of cleaved (cl)-caspase 3. At E13.5, all ventricles of *Snip1*^{Nes}-KO displayed strong induction of cl-caspase 3, accompanied by loss of NPCs (Fig 1d-g). Given that cl-caspase 3 signals were enriched in the subventricular zones (SVZs) of neuroepithelia, where most intermediate progenitors reside, we examined the markers of intermediate progenitors Tbr2 and Insm1. Compared with the control sibling, Tbr2 and Insm1 were markedly reduced in *Snip1*^{Nes}-KO neuroepithelia (Fig 1h-i). E13.5 brain undergoes massive neurogenesis and therefore, we next examined the immature neuron marker Tuj1. The relative thickness of the Tuj1-positive immature neuron region did not significantly differ between the *Snip1*^{Nes}-KO and control at E13.5 (Fig 1j-k). These data suggest that during E13.5–E15.5, a combination of robust apoptosis accompanied by differentiation to immature neurons leads to depletion of NPCs and intermediate progenitors. We concluded that Snip1 suppresses apoptosis in NPCs and intermediate progenitors in the developing brain.

Depletion of Snip1 in NPCs causes rapid onset of apoptosis throughout the developing brain

To study the temporal dynamics of apoptosis in the *Snip1*^{Nes}-KO brain, we examined cl-caspase 3 in the E11.5 embryos. By E11.5, cl-caspase 3 signals were detected throughout the *Snip1*^{Nes}-KO brain (Fig 2a-d). As *Nes*::Cre is turned on by E10.5 (Sclafani et al., 2006), Snip1 depletion likely induces apoptosis within 24 hours. The quantification of Sox2-positive cells in lateral, third, and fourth ventricles revealed a strong reduction of NPCs in the fourth ventricle (Fig 2e). Hereafter, we focused our analyses of lateral and third ventricles to study apoptosis control by Snip1.

We used *Emx1*::Cre, which turns on by E9.5 (Gorski et al., 2002), to deplete Snip1 in NPCs of the dorsal telencephalon. The *Snip1*^{Emx1}-KO embryos showed strong induction of apoptosis, loss of Tbr2-positive intermediate progenitors, and dysplasia of the forebrain (Fig 2f-g). These findings support that in the developing murine brain, strong apoptosis induction and brain dysplasia are independent of *Nes*::Cre and specific to Snip1 depletion. Taken together, these data led us to conclude that Snip1 is required for an anti-apoptosis and pro-survival mechanism in NPCs and intermediate progenitors.

Snip1 suppresses the intrinsic apoptosis program

To examine the molecular underpinnings of the apoptosis induction in *Snip1*^{Nes}-KO NPCs, we performed RNA-sequencing (RNA-seq) of Sox2-positive NPCs sorted from E13.5 *Snip1*^{Nes}-KO and sibling controls (Fig 3a, Supp Fig 4a). We analyzed genes with count per million (CPM) values >1 in either control or *Snip1*^{Nes}-KO NPCs. Using the criteria of false discovery rate (FDR) of <0.05 to compare 4-replicate datasets each from control and *Snip1*^{Nes}*-KO* NPCs, we identified 1210 upregulated genes and 1621 downregulated genes in *Snip1*^{Nes}-KO (Fig 3b, Supp Fig 4b). Gene set enrichment analysis (GSEA) revealed that upregulated genes in *Snip1*^{Nes}-KO NPCs were enriched in functions related to apoptosis, H3K27me3 or bivalent promoters in NPCs and the brain, midbrain markers, spliceosomal small nuclear ribonucleoprotein particles, and signaling pathways involving TNF, IGF, TGFβ, and Hedgehog (Fig 3c). Downregulated genes in *Snip1*^{Nes}-KO NPCs were enriched in functions related to forebrain and cortex development, CNS neuron differentiation, chromosome segregation, NPC proliferation, axonogenesis, replication fork, and signaling pathways involving TLR and Rho (Fig 3d).

As intrinsic and extrinsic apoptosis signatures were enriched in upregulated genes in *Snip1*^{Nes}-KO NPCs (Fig 3c), we examined the activation of these 2 pathways. IF showed little expression of cl-caspase 8, an effector of the extrinsic apoptosis pathway (Boldin et al., 1996; Muzio et al., 1996); Supp Fig 4c) but strong increases of cl-caspase 9, an effector of the intrinsic apoptosis pathway (Bronstein et al., 2017; Li et al., 1997; Srinivasula et al., 1998), throughout the neuroepithelia of ventricles (Fig 3e).

Next, we used inhibitors of caspases 8 and 9 and FACS of FAM-DEVD-FMK (probe to cl-caspase 3; (Bedner et al., 2000; Smolewski et al., 2001)) to show that whereas inhibition of caspase 8 modestly altered apoptosis, inhibition of caspase 9 / the intrinsic apoptosis pathway robustly reduced apoptosis in the *Snip1*^{Nes}-KO NPCs (Fig 3f-g, Supp Fig 4d).

GSEA results showed that downregulated genes in the *Snip1*^{Nes}-KO NPCs were enriched in forebrain developmental programs. IF revealed that although the *Snip1*^{Nes}-KO forebrain tissues displayed severe thinning as a consequence of apoptosis, the forebrain marker Foxg1 and the mid/hindbrain marker Otx2 were similarly detected between the control and *Snip1*^{Nes}-KO brains (Supp Fig 4e). These data suggest that Snip1 depletion did not alter forebrain specification. Additional follow-up IF analyses to the GSEA results detected little to no DNA damage (Supp Fig 4f-g), but strong increases of p53 activation (Supp Fig 4h-i), suggesting that the *Snip1*^{Nes}-KO embryo displayed dysregulated control of p53-mediated intrinsic apoptosis. We propose that Snip1 primarily suppresses the intrinsic apoptosis as part of a neurodevelopmental program.

Other enriched sets of downregulated genes in the *Snip1*^{Nes}-KO NPCs were related to the self-renewal control (Fig 3d). Characterization of the *Snip1*^{Nes}-KO NPCs *in vitro* showed that, compared with control, cultured *Snip1*^{Nes}-KO NPCs had reduced Sox2 expression (Supp Fig 5a). By allowing NPCs to form neurospheres in suspension and through serial passages, we found that neurosphere number and area were significantly lower in *Snip1*^{Nes}-KO compared with control (Supp Fig 5b-d). Lentiviral human SNIP1 (85% identity) expression was sufficient to rescue self-renewal in cultured *Snip1*^{Nes}-KO NPCs (Supp Fig 5e-f), suggesting functional conservation of Snip1. These findings suggest that Snip1 is required for the self-renewal in NPCs.

Snip1 directly regulates genetic programs including intrinsic apoptosis, cell cycle, and cortical development

GSEA revealed that the upregulated genes in the *Snip1*^{Nes}-KO NPCs were strongly enriched in the intrinsic apoptosis pathway (Fig 4a). To determine whether Snip1 proteins directly bind gene loci to regulate their expression, we profiled the genome-wide distribution of Snip1 by CUT&RUN(Skene and Henikoff, 2017) in *Snip1*^{Nes}-KO and sibling control NPCs (purified by Sox2-GFP FACS). We observed strong enrichment of Snip1 at promoters of *Cdkn1a*, *Trp73*, and *Msx1* (Fig 4b; upregulated in *Snip1*^{Nes}-KO), as well as *Hmgb2*, *Tbr2*, and *Lhx6* (Fig 4c; downregulated in *Snip1*^{Nes}-KO). Using SICER (Xu et al., 2014) and FDR<0.05 to compare 2 datasets each from control and *Snip1*^{Nes}-KO, we identified -12,621 Snip1-bound regions in control NPCs and only 792 regions in *Snip1*^{Nes}-KO NPCs (Supp Fig 6a). Visualization of the 12,621 sites by heatmaps showed highly reduced Snip1 CUT&RUN signals in *Snip1*^{Ne}-KO (Supp Fig 6b). These differences showed the high specificity of Snip1 CUT&RUN in NPCs.

Approximately 64.2% of Snip1-bound peaks were within promoters (within 2kb of transcription start sites), 4.1% were located in exons, 17.1% in introns, 0.8% in transcription termination sites, 7.6% in 5′ distal (2-50kb from a gene) regions, 2.6% in 3′ distal (2-50kb from a gene) regions, and 3.6% in intergenic (beyond 50kb from a gene) regions (Supp Fig 6c). Only 13.8% of Snip1-bound peaks were located distal to a gene (Supp Fig 6c).

Remarkably, of the 44 genes in the intrinsic apoptosis pathway that were upregulated in *Snip1*^{Nes}-KO, 22 loci were bound by Snip1 at the promoters in the control NPCs (p = 2.2e-42; Fig 4d). This prompted us to further examine Snip1 targets that became differentially expressed in *Snip1*^{Nes}-KO. GSEA showed that Snip1 targets that became upregulated in *Snip1*^{Nes}-KO were enriched in p53 pathway, medulla, and apoptosis (Fig 4e), whereas Snip1 targets that became downregulated in *Snip1*^{Nes}-KO were enriched in G2M checkpoint, cortical development, and cellular component disassembly upon apoptosis (Fig 4f). These data suggest that Snip1 directly regulates genetic programs crucial to apoptosis control, cell cycle, and cortical development.

Snip1 binds to the PRC2 complex and co-occupies PRC2 targets on chromatin of NPCs

We noticed a strong correlation between upregulated genes and lower H3K27me3 occupation, whereas downregulated genes had higher H3K27me3 occupation in *Snip1*^{Nes}-KO (Fig 4e-f). Furthermore, upregulated genes were enriched with known high-CpG-density promoters occupied by H3K27me3 in the embryonic murine brain (Meissner et al., 2008) and high-CpG-density promoters with bivalent (H3K27me3 and H3K4me3) marks in mouse NPCs (Mikkelsen et al., 2007) (Fig 4g-h). This prompted us to investigate the interactions between Snip1 and H3K27 methyltransferase PRC2. Anti-Snip1 antibody co-immunoprecipitated with known PRC2 subunits Jarid2, Suz12, and Ezh2, but not the negative control Rbbp5 in the NPC nuclear extract (Fig 4i). Anti-Jarid2 or Ezh2 antibody co-immunoprecipitated Snip1 and other PRC2 subunits but not the negative control Rbbp5 in the NPC nuclear extract (Fig 4j-k). Anti-p300 or Cbp antibody failed to co-immunoprecipitate with Snip1, suggesting that in NPCs, their interaction is minimal (Supp Fig 6d-e). These data provided the rationale to examine the occupation of Snip1 with H3K27me3 on chromatin and the functional interaction of Snip1 with PRC2.

Snip1 functionally interacts with PRC2 to modulate the intrinsic apoptosis program

We next tested whether Snip1 interacts cooperatively or antagonistically with PRC2 to regulate NPC survival. To genetically deplete the PRC2 core subunit Eed, we used *Nes*:Cre to excise exons 3 to 6 of *Eed* in *Eed*^{Nes}-KO and *Snip1*^{Nes}-*Eed*^{Nes}-dKO (Supp Fig 7a-b). The Eed depletion alone was not sufficient to induce apoptosis or alter self-renewal of NPCs (Supp Fig 7c-e). Compared with *Snip1*^{Nes}-

KO, *Snip1*^{Nes}-*Eed*^{Nes}-dKO mouse brains had similar proportions of Tbr2- or Insm1-positive intermediate progenitors and Tuj1-positive immature neurons (Fig 5a-c). Quantification of at least 5 embryos showed that compared with *Snip1*^{Nes}-KO brains, *Snip1*^{Nes}-*Eed*^{Nes}-dKO brains had significantly fewer cl-caspase 3-positive cells and more Sox2-positive NPCs (Fig 5d-e). These results suggest that Eed depletion in the *Snip1*^{Nes}-KO embryonic brain reduces apoptosis and rescues NPCs. Therefore, PRC2 and Snip1 physically and functionally interact to regulate the intrinsic apoptosis program during embryonic brain development.

DISCUSSION

In the developing brain, neural cells are prone to undergo apoptosis (Bieberich et al., 2001; Blaschke et al., 1996; Sommer and Rao, 2002; Thomaidou et al., 1997). Our study advances this understanding by uncovering the crucial anti-apoptosis/pro-survival role of Snip1, its molecular activities, and its interaction with PRC2 to modulate caspases 9 and 3 activities. By showing that Snip1 protein binds genes involved in the intrinsic apoptosis pathway and suppresses their expression in NPCs, we illuminate the programming of pro- and anti-apoptosis decisions in NPCs that are essential to brain development. Initially, given our finding that Snip1 suppresses intrinsic apoptosis, we had hypothesized a cooperative relationship between Snip1 and PRC2 in regulating intrinsic apoptosis. Therefore, the rescue of *Snip1*^{Nes}-KO NPCs by Eed/PRC2 depletion came as an intriguing surprise and suggests an antagonistic relationship between Snip1 and PRC2 in regulating apoptosis. Future profiling of chromatin dynamics in *Snip1*^{Nes}-KO versus control NPCs will clarify the mechanistic details.

Caspase 9 and intrinsic apoptosis in brain development has been little understood, despite the human genetic evidence connecting loss of function in caspase 9 to neural tube defects (Liu et al., 2018; Spellicy et al., 2018; Zhou et al., 2018) and pediatric brain tumors (Ozdogan et al., 2017; Ronellenfitsch et al., 2018). Global KO of either caspase 3 or 9 in mice leads to prenatal death with brain malformation, including neural tube closure defect and exencephaly (Hakem et al., 1998; Kuida et al., 1998; Kuida et al., 1996). These findings point to a conserved requirement of caspase 3 and 9 for brain development. Our study implicates the essential roles of Snip1 and PRC2 in dampening the activities of caspase 9 and caspase 3 in order to balance the growth, division, and death of NPCs.

The role of Snip1 in apoptosis has been implicated in past studies (Fernandez et al., 2018). Snip1 depletion by morpholino to induce acridine orange (apoptosis detection) signals in zebrafish embryo suggests that the anti-apoptosis function of Snip1 is conserved (Fernandez et al., 2018). In this study, we show that robust induction of cl-caspase 3 and cl-caspase 9 contributes to severe brain dysplasia in the *Snip1*^{Nes}-KO murine brain. By profiling the chromatin occupancy of Snip1, we uncover

its direct role in suppressing intrinsic apoptosis through interacting with PRC2. The Snip1 CUT&RUN data identified 22 genes that are involved in intrinsic apoptosis and directly regulated by Snip1. Further examination is needed to uncover how these genes orchestrate the caspase 9-dependent apoptosis downstream of the Snip1-PRC2 axis.

PRC2 maintains the self-renewal of NPCs by suppressing gene expression for neurogenesis (Evans et al., 2020). Compared to control NPCs, *Snip1*^{Nes}-KO NPCs had reduced expression of genes involved in chromosome segregation, NPC proliferation, and replication fork. In our cell culture system, *Snip1*^{Nes}-KO NPCs diminished the number and the size of neurospheres over time. These observations implicate the potential role of Snip1 in aiding the proper cell cycle progression of NPCs through gene regulation. Altogether, we unveiled the multiple developmental roles of Snip1 via chromatin-mediated gene regulation: suppression of p53 and its targets, restricting hindbrain lineage including medulla, promoting the G2M checkpoint, and promoting cortical development. These discoveries also suggest that Snip1 and Snip1–PRC2 interaction are multifunctional in the developing brain. Clinical relevance of the *SNIP1* gene has been recently documented. Homozygous 1097A>G (Glu366Gly) variant on human *SNIP1* has been linked to a neurodevelopmental disorder having clinical features including skull dysplasia, global developmental delay, and intellectual disability and seizure (Ammous et al., 2021; Puffenberger et al., 2012). Our findings on the Snip1-PRC2 interaction in suppressing apoptosis and promoting neural development in the developing brain hold promise for better understanding of the neurodevelopmental disorders caused by SNIP1 mutations and PRC2 dysregulation.

ACKNOWLEDGEMENTS

The authors thank V. Shanker for editing the manuscript; J. Houston and K. Lowe for FACS; M. Evans, I. Lam, and I. Chapman for experimental assistance. RNAscope was performed by the Comparative Histology Core at SJCRH. Sequencing was performed at the Harwell Center for Biotechnology and images were acquired at the Cell & Tissue Imaging Center, both of which are supported by SJCRH and NCI P30 (CA021765). M.N.D, Y.F., and B.X. are supported by NCI P30 grant (CA21765). This work is funded by the American Lebanese Syrian Associated Charities, American Cancer Society (132096-RSG-18-032-01-DDC), and NIH (1R01GM134358-01). The content is solely the responsibility of the authors and does not necessarily represent the official views of the National Institutes of Health. The funders had no role in study design, data collection and analysis, decision to publish, or preparation of the manuscript.

AUTHOR CONTRIBUTIONS

Y.M.: Most experiments, data analyses, and manuscript writing. M.N.D. and B.X.: bioinformatics analyses. K.L.: mouse harvesting and rescue by lentiviral Snip1. P.S.: ideas on studying apoptosis and inhibitor assays. N.C. and H.C.: mouse breeding and DNA constructs. Y.F.: supervision of bioinformatics analyses. J.C.P.: project design, data analyses, and manuscript writing with inputs from all authors.

COMPETING INTERESTS

The authors declare no competing interests.

METHODS

Buffers

PBS: 137 mM NaCl, 2.7 mM KCl, 10 mM phosphate buffer (pH 7.4)

PBST: PBS with 0.1% Triton X-100

HEPM (pH 6.9): 25 mM HEPES, 10 mM EGTA, 60 mM PIPES, 2 mM $MgCl_2$

IF blocking buffer: 1/3 Blocker Casein (Thermo Scientific 37528), 2/3 HEPM with 0.05% Triton X-100

Buffer A: 10 mM HEPES (pH 7.9), 10 mM KCl, 1.5 mM $MgCl_2$, 0.34 M sucrose, 10% glycerol

Buffer D: 400 mM KCl, 20 mM HEPES, 0.4 mM EDTA, 20% glycerol

iDISCO PTx.2: PBS with 0.2% Triton X-100

iDISCO PTwH: PBS with 0.2% Tween-20 and 10 µg/mL heparin

iDISCO Permeabilization solution: PTx.2 with 306 mM glycine and 20% DMSO

iDISCO Blocking solution: PTx.2 with 6% donkey serum and 10% DMSO

CUT&RUN Binding buffer: 20 mM HEPES-KOH (pH 7.9), 10 mM KCl, 1 mM $CaCl_2$, 1 mM $MnCl_2$

CUT&RUN Wash buffer: 20 mM HEPES (pH 7.5), 150 mM NaCl, 0.5 mM spermidine, Protease Inhibitor Cocktail (Sigma-Aldrich
11873580001)

CUT&RUN Digitonin block buffer: CUT&RUN Wash buffer with 2 mM EDTA and 0.05% digitonin

CUT&RUN 2X Stop buffer stock: 340 mM NaCl, 20 mM EDTA, 4 mM EGTA, 0.02% digitonin

CUT&RUN Stop buffer: Into 1 mL of 2X Stop buffer stock, add 5 µL of 10 mg/mL RNase A and 133 µL of 15 mg/mL GlycoBlue™ Coprecipitant (Thermo Fisher Scientific AM9516)

Antibodies used in this study are listed in Supplementary Table 1.

Animals

All animal experiments were approved by the Institutional Animal Care and Use Committee at St. Jude Children's Research Hospital and were conducted in accordance with ethical guidelines for animal research. To generate conditional knockout embryos, we used the Cre/lox system. *Snip1*-tm1a (Infrafrontier/EMMA 04224) were first crossed with *Actin*-FLPe to generate the *Snip1*-flox line. To genetically label mouse NPCs, *Snip1*-flox; *Nestin*-Cre mice were crossed with *Sox2*-eGFP transgenic mice. Embryos were harvested at embryonic days as indicated in the figures or text. For all the animal experiments, both sexes were included, and knockout embryos were compared to their sibling control littermates. The following mouse lines used in this study and genotyping primers and conditions are shown in Supplementary Table 2:

Snip1-tm1a: B6Dnk;B6N-*Snip1*<tm1a(EUCOMM)Wtsi>/H (Infrafrontier/EMMA 04224)
Eed-flox: B6;129S1-*Eed*^{tm1Sho}/J (JAX Stock 022727) (Yu et al., 2009)
Smad4-flox: *Smad4*$^{tm2.1Cxd}$/J (Jackson 017462) (Yang et al., 2002)
Ep300-flox: 129S.129P2(B6)-*Ep300*^{tm2Pkb}/J **(**a gift from Dr. Charles Mullighan at St. Jude Children's Research Hospital, JAX Stock 025526) (Kang-Decker et al., 2004)
Cbp-flox: B6.Cg-*Crebbp*^{tm1Jvd}/J **(**a gift from Dr. Charles Mullighan at St. Jude Children's Research Hospital, JAX Stock 025178) (Kasper et al., 2006)
Actin-FLPe: B6;SJL-Tg(*ACT*FLPe)9205Dym/J (a gift from Dr. Peter McKinnon at St. Jude Children's Research Hospital, JAX Stock 003800) (Rodriguez et al., 2000)
Nestin-Cre: B6.Cg-Tg(*Nes*-Cre)1Kln/J (JAX Stock 003771) (Tronche et al., 1999)
Emx1-Cre: B6.129S2-Emx1$^{tm1(cre)Krj}$/J (a gift from Dr. Peter McKinnon at St. Jude Children's Research Hospital, JAX Stock 005628) (Lee et al., 2012)
Sox2-eGFP: B6;129S1-*Sox2*^{tm1Hoch}/J (JAX Stock 017592) (Arnold et al., 2011)

Isolation and Culturing of Mouse NPCs

To obtain mouse brain cells, embryos at an indicated embryonic day were dissected out from the uterus and visceral yolk sac. A part of the tail or limbs was collected for genotyping. Brains were dissected from embryos under the dissection microscope in cold 1x PBS. Then, 300 µL Dulbecco's Modified Eagle's Medium (DMEM) (ATCC 30-2002) and 150 µL of 10 mg/mL collagenase Type II (Worthington LS004176) were added to each brain and incubated for 5-10 min at 37 °C. After centrifugation at 1000 xg for 3 min, the tissue was incubated with 500 µL 0.25% Trypsin-EDTA (ThermoFisher 25200056) for 5 min at 37 °C. Trypsinization was quenched with 500 µL DMEM supplemented with 10% fetal bovine serum (FBS) and pelleted by centrifugation at 1000 xg for 3 min. Cells were resuspended in 500 µL of

NPC culture media (NeuroCult™ Proliferation Media; STEMCELL Technologies 05702) supplemented with 30 ng/mL human recombinant epidermal growth factor (rhEGF) (STEMCELL Technologies 78006) and filtered through a 40 µm filter (Fisherbrand™ 22-363-547) to obtain single cells. To collect NPCs, the dissociated brain cells were cultured in ultra-low attachment 6-well plates (Corning® Costar® CLS3471) in the NPC culture media at 37 °C. NPCs formed neurospheres in suspension. For passaging, neurospheres were incubated with Accutase™ (STEMCELL Technologies 07920) for 5 min in the 37 °C bead bath and then dissociated by pipetting. After adding an equal volume of the NPC culture media, dissociated cells were centrifuged at 500 xg for 5 min. Cells were then grown in the NPC culture media either in suspension in the ultra-low attachment 6-well plates or on matrigel (Corning™ 354230) coated plates. The medium was changed every 2 to 3 days. For collecting uncultured NPCs, brain cells were sorted by fluorescence-activated cell sorting (FACS) using Sox2-eGFP or NeuroFluor™ CDr3 (STEMCELL Technologies 01800).

Neurosphere Assay

1 X 10^4 NPCs were seeded into each well of ultra-low attachment 6-well plates. For each experimental group, three wells were set up in replicates. The NPCs were grown in the NPC culture media at 37 °C for 5 days with 250 µL of media added every 2 days. After 5 days of culturing, at least 8 images of neurospheres per well were captured with ZEISS AxioObserver D1 at 5x magnification. The area and the number of neurospheres were quantified by using FIJI. To generate clean binary images, images were processed with “Process” -> “Find edges” followed by “Image” -> “Adjust” -> “Threshold”. After inverting the images, the number and the area of the neurospheres were obtained by selecting “Analyze” -> “Analyze particles”. If multiple neurospheres were too close for the software to quantify individually, one of the two methods was applied after generating the binary images: manual quantification by drawing the outline of each neurosphere and selecting “Analyze” -> “Measure”, or computationally separating the neurospheres by selecting “Process” -> “Binary” -> “Fill Holes,” followed by “Process” -> “Binary” -> “Watershed”.

Inhibitor Treatment and FACS-Based Cell Death Assay

The 5 X 10^5 NPCs from control and homozygous Snip1-flox embryos were seeded onto each well of matrigel-coated 6-well plates. On the following day, cells were incubated with mCherry-Cre lentivirus (Vector Core Lab at St. Jude Children’s Research Hospital) for 8 h, washed twice with 1X PBS, and cultured for 3 days. To quantify the population of cells with active caspases 3 and 7, cells were incubated at 37 °C with reconstituted FAM-FLICA® at a 1:300 dilution (ImmunoChemistry Technologies 94) for 30 min. Cells were fixed in a 4% formaldehyde solution at room temperature for 15 min and

washed twice with 1X PBS. FAM-FLICA–positive cells were quantified by FACS (Excitation: 492 nm, Emission: 520 nm). FACS data were analyzed by FlowJo. To test the involvement of BMP/TGFβ and NFκB signaling pathways in cell death, Galunisertib (an inhibitor of TGFβ receptor I), K02288 (an inhibitor of BMP type I receptors), LDN-193189 (another inhibitor of BMP type I receptors), IKK-16 (an inhibitor of IκB kinases), BAY11-7082 (an inhibitor of IκB-α kinase) and JSH-23 (an inhibitor of NFκB nuclear translocation) were dissolved in DMSO at the concentration of approximately 1mM and stored in -80 °C (Compound Management Center at St. Jude Children's Research Hospital). To examine whether cell death is via activation of caspase 8 or 9, Z-IETD-FMK (a caspase 8 inhibitor) and Z-LEHD-FMK TFA (a caspase 9 inhibitor) were dissolved in DMSO at 50mM and stored in -80 °C (Compound Management Center at St. Jude Children's Research Hospital). After cells were incubated with mCherry-Cre lentivirus for 8 h, these compounds were added at a series of concentrations and incubated for 3 days before FACS analysis. Similarly, to test the involvement of chromatin modifiers in cell death, the Ezh2 inhibitor GSK126 (Cayman Chemical 15415) and the p300/Cbp inhibitor, A-485 (Cayman Chemical 24119) were dissolved in DMSO to stock concentrations of 4.75 mM and 18.6 mM, respectively, and stored in -80 °C. NPCs were pre-treated with GSK126 or A-485 at 2 μM for two days and seeded for the transduction with mCherry-Cre lentivirus. For all the inhibitor treatment assays, medium with the inhibitors was changed every 2 days.

Subcellular Protein Extraction

After washing cells once with 1x PBS, they were resuspended in 2x volume of Buffer A supplemented with PI, 1 mM DTT, and 0.1% TritonX-100 and placed on ice for 5 min. Cells were centrifuged at 1750 x g for for 2 min at 4 °C and supernatant was collected as the cytoplasmic fraction. The nuclear pellet was then resuspended in 1x volume of Buffer D supplemented with PI, 1 mM DTT, and 0.1% TritonX-100 and placed on ice for 30 min (If volumes were large, tubes were rotated at 4 °C). The lysate was centrifuged at 1750 x g for for 2 min at 4 °C and supernatant was collected and diluted with an equal volume of H_2O (nuclear fraction). The chromatin pellet was washed once with cold 1x PBS and resuspended in 1x volume of 0.1 N HCl at 4 °C overnight (O/N). The chromatin fraction was centrifuged at 1750 x g for 2 min at 4 °C, the supernatant was collected, and 1/10 volume of 1.5 M Tris-HCl (pH 8.8) was added to neutralize the acid. For whole-cell lysate extraction, cells were washed once with 1X PBS and resuspended directly in 2x volume of Buffer D supplemented with PI, 1 mM DTT, and 0.1% TritonX-100.

Co-Immunoprecipitation

Nuclear proteins were extracted as above. Then, 15 µL of protein A and 15 µL of protein G Dynabeads™ (Invitrogen 10002D and 10004D) were washed once with 1x PBST. For pre-bound co-immunoprecipitation, the beads were resuspended in 100 µL of HEPM and 4 µg primary antibody was added. The tube was gently shaken at room temperature for 2 h. The beads were washed once with 1x PBST, and approximately 2.5 mg of nuclear extract was added to the antibody-prebound beads and the tube was rotated at 4 °C for 2.5-4 h. Beads were then washed three times with 1x PBST and proteins were eluted with 0.1 M glycine (pH 2.3) at room temperature. Eluates were neutralized with 1/10 volume of 1.5 M Tris-HCl (pH 8.8). For co-immunoprecipitation with free antibodies, approximately 2.5 mg of nuclear extract was incubated with 4 µg of primary antibody and rotated at 4 °C for 4 h. Beads were then added to the extract and gently shaken for 1 h at room temperature. The same washing and elution steps were performed as for the pre-bound co-immunoprecipitation.

Western Blotting (WB)

For SDS-PAGE, resolving and stacking gels were prepared using the following composition. Resolving gels: 6-12% ProtoGel (National Diagnostics EC8901LTR), 0.375 M Tris-HCl (pH 8.8), 0.1% SDS, 0.1% ammonium persulfate (APS) and 0.1% TEMED (National Diagnostics EC-503). Stacking gels: 3.9% ProtoGel, 0.125M Tris-HCl (pH 6.8), 0.1% SDS, 0.05% APS, and 0.12% TEMED. After proteins were separated by SDS-PAGE, they were transferred onto a 0.45 µm nitrocellulose membrane (Bio-Rad 1620115) by the semi-dry transfer system. Membranes were blocked with 2% BSA in HEPM for 1h at room temperature and incubated in primary antibodies diluted in the 2% BSA at 4 °C O/N. On the following day, the membrane was washed three times with 1x PBST and incubated in IRDye®-conjugated secondary antibodies (LI-COR) or Clean-Blot™ IP detection reagent (Thermo Scientific 21230) on a shaker for 1 h at room temperature. The membrane was washed three times with 1x PBST and immediately imaged on an Odyssey® Fc imaging system (LI-COR). The membrane stained with Clean-Blot™ IP detection reagent (product info) was treated with SuperSignal™ West Pico PLUS Chemiluminescent Substrate (Thermo Scientific 34577) for at least 5 min at room temperature before imaging. Signals were quantitated using the Image Studio™ software (version 1.0.14; LI-COR).

BrdU Administration

Mice were administered 5-bromo-2′-deoxyuridine (BrdU, Sigma-Aldrich B5002) reconstituted in sterile 1x PBS by intraperitoneal injection at a dose of 50 mg/kg. After 5 h, the mice were sacrificed for dissection.

Cryosection

Mouse embryos at an indicated embryonic day were fixed in 4% formaldehyde at 4 °C O/N. The embryos were washed three times in 1x PBS for 30 min at room temperature and placed in 15% sucrose diluted in 1x PBS at room temperature until the embryos sank at the bottom of the tube. Then, the embryos were moved to a 30% sucrose solution and incubated at room temperature until the embryos sank. The embryos were then treated in the embedding medium Tissue-Tek® O.C.T. Compound (Sakura Finetek USA INC 4583) to rinse the residual sucrose. Each embryo was mounted in the embedding media in a cryosection mold placed on dry ice and 12-μm sagittal cryosections were obtained (Leica CM3050 S).

Immunofluorescence (IF)

For cryosections, the slides were permeabilized by incubating with 1x PBST at 4 °C O/N. After drawing the outline of the staining area with a hydrophobic barrier pen (ImmEdge® H-4000), the slides were blocked with IF blocking buffer for 2-3 h at room temperature. Primary antibodies were diluted at the optimized concentration in the IF blocking buffer and incubated at 4 °C O/N. Sections were washed three times with 1x PBST and fluorescent dye–conjugated Alexa Fluor secondary antibodies (Invitrogen) diluted at 1:500 in the IF blocking buffer were added for a 2-3 h incubation at room temperature in the dark. Sections were washed three times with 1x PBST and incubated in 1 mg/mL DAPI (Sigma-Aldrich D9542) diluted at 1:500 in 1x PBS at room temperature for 1 h. Finally, the sections were washed once with 1x PBS and mounted with ProLong™ Gold Antifade Mountant (Life Technologies P10144). For detecting BrdU, the tissue was permeabilized as above and rinsed with 1x PBS for 5 min at room temperature. Then, the tissue was treated with 2 N HCl for 1 h at room temperature. Sections were washed multiple times with 1x PBS to remove all traces of HCl and were blocked and stained as above. Images were acquired with a Nikon C2 laser scanning confocal microscope.

Image Analysis

The number of cells on the IF images were quantified by FIJI. All the images were first converted to an 8-bit grayscale. In the automatic nuclei counter plugin (ITCN) of FIJI, for each primary antibody, “Width”, “Minimum Distance” and “Threshold” were set manually based on the area and the intensity of the signal on the representative images. The same parameters on ITCN were applied for control and experimental groups. For each group, five images were analyzed.

iDISCO

We performed iDISCO clearing method using the protocol developed by the Tessier-Lavigne lab (Renier et al., 2014). In brief, mouse embryos at an indicated embryonic day were fixed in 4% formaldehyde and washed in 1X PBS (see Cryosection section). Samples were first dehydrated by incubating them for 1 hr each with the increasing concentrations of methanol at 20%, 40%, 60%, 80%, and 100% at room temperature. Samples were then incubated in 66% dichloromethane (DCM)/ 33% methanol O/N. Samples were washed twice in 100% methanol, pre-chilled at 4 °C and incubated with 5% H_2O_2 in methanol at 4 °C O/N. Samples were then rehydrated by incubating them for 1 hr each with the decreasing concentrations of methanol at 80%, 60%, 40%, 20% and 1X PBS at room temperature. Samples were washed twice in PTx.2 for 1 hr each. For immunolabeling, samples were incubated in a permeabilization solution at 37 °C for 2 days and blocked in Blocking solution at 37 °C for 2 days. Primary antibodies diluted in PTwH supplemented with 5% DMSO and 3% donkey serum were incubated at 37 °C for 3-4 days. Samples were moved to the freshly diluted antibodies and incubated for another 3 - 4 days. Samples were washed in PTwH for 4-5 times for the entire day and incubated with the secondary antibodies diluted in PTwH supplemented with 3% donkey serum at 37 °C for 3-4 days. Again, the antibodies were replaced with freshly diluted antibodies and incubated for an additional 3-4 days. Samples were washed in PTwH for 4-5 times for the entire day. For clearing, samples were first dehydrated with methanol as described above and treated with 66% DCM/ 33% methanol for 3 hours at room temperature. Samples were washed twice with 100% DCM to rinse off methanol and incubated with dibenzyl ether to clear the tissues. Images were acquired with a LaVision light sheet microscope.

RNAscope VS Duplex Assay

To detect the expression pattern of different transcripts in the brain, mouse embryos at an indicated embryonic day were fixed in 10% neutral-buffered formalin (NBF) at room temperature. Fixed embryos were paraffin-embedded and sectioned at a thickness of 4 μm. RNA probes were designed and purchased from ACDBio; Snip1 probe targeting 1270-2274 bp of NM_001356560.1 and Eomes/Tbr2 probe targeting 1289-2370 bp of NM_010136.3 (Cat. 429649-C2). Sectioning and *in situ* hybridization (ISH) were done by the Comparative Histology Core at St. Jude Children's Research Hospital by following manufacturer's instructions. Brightfield images were acquired with Keyence BZ-X700.

RNA Extraction and Reverse Transcription

Total RNA was extracted from FACS-sorted cells using TRIzol reagent (Invitrogen™ 15596026) and Direct-zol™ RNA Microprep (Zymo Research R2062) by following manufacturer's instructions. DNA digestion with DNase I was also performed as part of the RNA extraction. cDNA was prepared with

500-1000 ng of total RNA using SuperScript™ IV VILO™ Master Mix (ThermoFisher 11766050) by following manufacturer's instructions.

Real-Time Quantitative PCR (RT-qPCR)

RT-qPCR was performed with PowerUp™ SYBR™ Green Master Mix (Applied Biosystems™ A25778) using Applied Biosystems QuantStudio 3. Primers are listed in Supplementary Table 3. Three technical replicates were set up for each gene target. For data analysis, $2^{-\Delta\Delta Ct}$ method, which compares the difference in the threshold cycle values of control and experimental samples, was used. The threshold cycle values of a gene of interest was normalized to that of the housekeeping gene *Gapdh*.

RNA-Seq analysis

Paired-end 100-cycle sequencing was performed on NovaSeq6000 sequencer by following the manufacturer's instructions (Illumina). Raw reads were first trimmed using TrimGalore (version 0.6.3) available at: https://www.bioinformatics.babraham.ac.uk/projects/trim_galore/ , with parameters '--paired --retain_unpaired'. Filtered reads were then mapped to the *Mus musculus* reference genome (GRCm38.p6 + Gencode-M22 Annotation) using STAR (version 2.7.9a) (Dobin and Gingeras, 2015) [PMID: 26334920]. Gene-level read quantification was done using RSEM (version 1.3.1) (Li and Dewey, 2011). To identify the differentially expressed genes between control and experimental samples, the variation in the library size between samples was first normalized by trimmed mean of *M* values (TMM) and genes with CPM < 1 in all samples were eliminated. Then, the normalized data were applied to linear modeling with the voom from the limma R package (Law et al., 2014). Gene set enrichment analysis (GSEA) was performed against using the MSigDB database (version 7.1), and differentially expressed genes were ranked based on the their $\log_2$(FC) * -$\log_{10}$(p-value) * mean expression (Liberzon et al., 2015; Subramanian et al., 2005).

CUT&RUN

Approximately 3×10^5 NPCs sorted for *Sox2*-eGFP were mixed with 3×10^4 *Drosophila* S2 cells per reaction. We performed CUT&RUN using the protocol developed by the Henikoff lab (Skene and Henikoff, 2017). In brief, Bio-Mag®Plus Concanavalin-A (Con A) coated beads (Bangs Laboratories BP531) were washed and activated with Binding buffer. Nuclei of NPCs with S2 spike-in were gently prepared (see Subcellular Protein Extraction section). Activated Con A beads and nuclei were then mixed and rotated for 5 min at room temperature. They were then blocked with Digitonin block buffer for 5 min at room temperature. 0.5-1 µg of primary antibody with 0.25 µg Spike-in antibody (Active Motif 61686) diluted in Digitonin block buffer was added to the bead-nuclei mixture and incubated for 3 hours

(histone marks) or O/N (the rest). Beads were washed three times with Digitonin block buffer and incubated with pA-MNase for 1 h at 4 °C. Beads were washed three times with Wash buffer and incubated in Wash buffer for 10 min on ice. The pA-MNase is activated by incubating the beads with 2 mM $CaCl_2$ for 25 min on ice and quenched by adding the Stop buffer. DNA was released from the beads by incubating them for 30 min and collected by centrifugation at 16,000 x g for 5 min at 4 °C. DNA was then isolated by using a phenol/chloroform extraction method. Libraries were constructed using ACCEL-NGS® 1S Plus DNA Library Kit by following the manufacturer's instructions (Swift Biosciences 10024). Purified libraries were analyzed with TapeStation (Agilent), using the High Sensitivity D1000 reagents (Agilent 5067-5585) before sequencing. IgG primary antibody was used as the negative control.

CUT&RUN Analysis

CUT&RUN libraries were sequenced on NovaSeq6000 sequencer and generated 50 bp paired-end reads. The reads were aligned to mouse mm10 genome reference and fruit fly dm6 genome reference by BWA (version 0.7.170.7.12, default parameter). Read counts were normalized by using the trimmed mean of *M* values (TMM) normalization method (Robinson and Oshlack, 2010) and applied to linear modeling with the voom package from the limma R package. Duplicated reads were marked by the bamsormadup from the biobambam tool (version 2.0.87) available at https://www.sanger.ac.uk/tool/biobambam/. Uniquely mapped reads were kept by samtools (parameter "-q 1 -F 1804," version 1.14). Fragments < 2000 bp were kept for peak calling and bigwig files were generated for visualization. SICER was used for peak identification. With SICR, we assigned peaks that were at the top 1 percentile as the high-confidence peaks and the top 5 percentile as the low-confidence peaks. Peaks of control and experimental groups were compared by the empirical Bayes method (eBayes function from the limma R package (Law et al., 2014)). For downstream analyses, heatmaps were generated by deepTools (Ramirez et al., 2014) and gene ontology was performed with Enrichr (Chen et al., 2013; Kuleshov et al., 2016).

Statistics and Reproducibility

Statistical analyses were performed using R 4.0.1 or Prism 9.0.2 (GraphPad Software). Parameters of statistical analyses such as the number of replicates and/or experiments (*n*), deviations, p-values, and types of statistics tests are included in the figures or figure legends. For all the *in vivo* experiments, at least three biological replicates were assessed. All *in vitro* assays were performed with at least two independent sample sets. Error bars on graphs represent the mean ±SEM.

MAIN FIGURES AND LEGENDS

Matsui_FIGURE 1

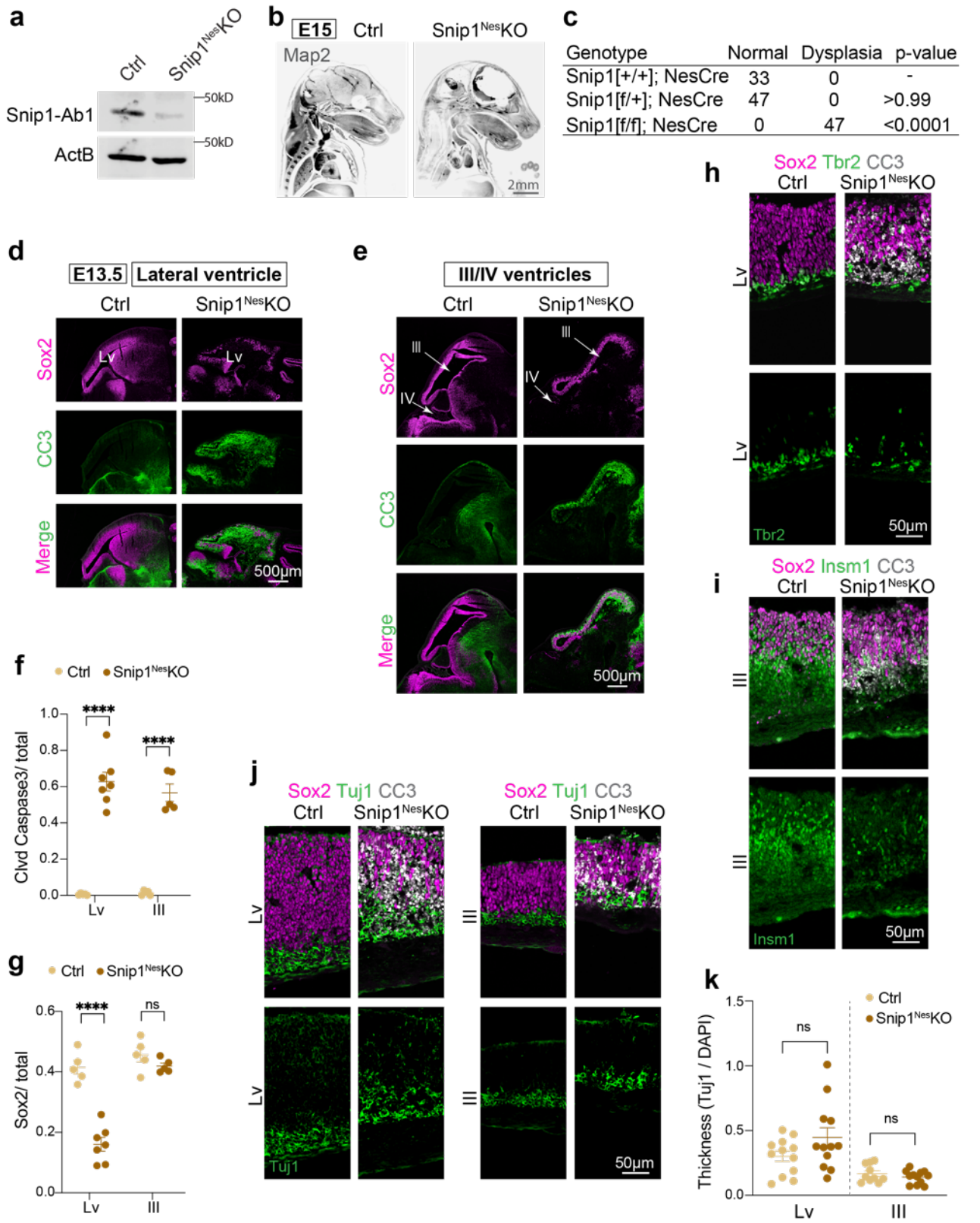

Fig. 1 Depletion of *Snip1* in NPCs causes brain dysplasia in mouse embryos.

a WB of control and *Snip1*^{Nes}-KO NPCs at E13.5. Snip1-Ab1; anti-Snip1 antibody from Proteintech.

b IF of Map2 in control and *Snip1*^{Nes}-KO embryos at E15. Embryos were cleared by the iDISCO method and imaged with light sheet microscopy. Bar, 2 mm.

c Penetrance of brain dysplasia in E13.5 embryos. Brain dysplasia was determined by thinning of the brain tissue. Statistical significance was calculated by Fisher's exact test.

d-e IF of Sox2 and cleaved caspase 3 (CC3) in sagittal cryosections of the E13.5 brain. Germinal zones around the lateral ventricle (Lv, forebrain) (**d**) and 3rd (midbrain) /4th (hindbrain) ventricles (**e**) were examined. Bar, 500 µm.

f-g Quantification of CC3-positive and Sox2-positive cells in the neuroepithelial lining of the ventricles of control and *Snip1*^{Nes}-KO embryos at E13.5. DAPI staining was used to count the total number of cells. Each data point represents one image. N=5 pairs of embryos. Data are presented as mean ± SEM and two-way ANOVA was used for statistical analysis. ns = not statistically significant; ****$p < 0.0001$.

h-j IF of Sox2 and CC3 overlayed with neural lineage markers, Tbr2, Insm1, or Tuj1 of the E13.5 brain. Bar, 50 µm.

k Thickness of the Tuj1-positive region relative to the entire cortical thickness. Each data point represents one image. N=4 pairs of embryos. Data are presented as mean ± SEM and unpaired t-test was used for statistical analysis. ns = not statistically significant.

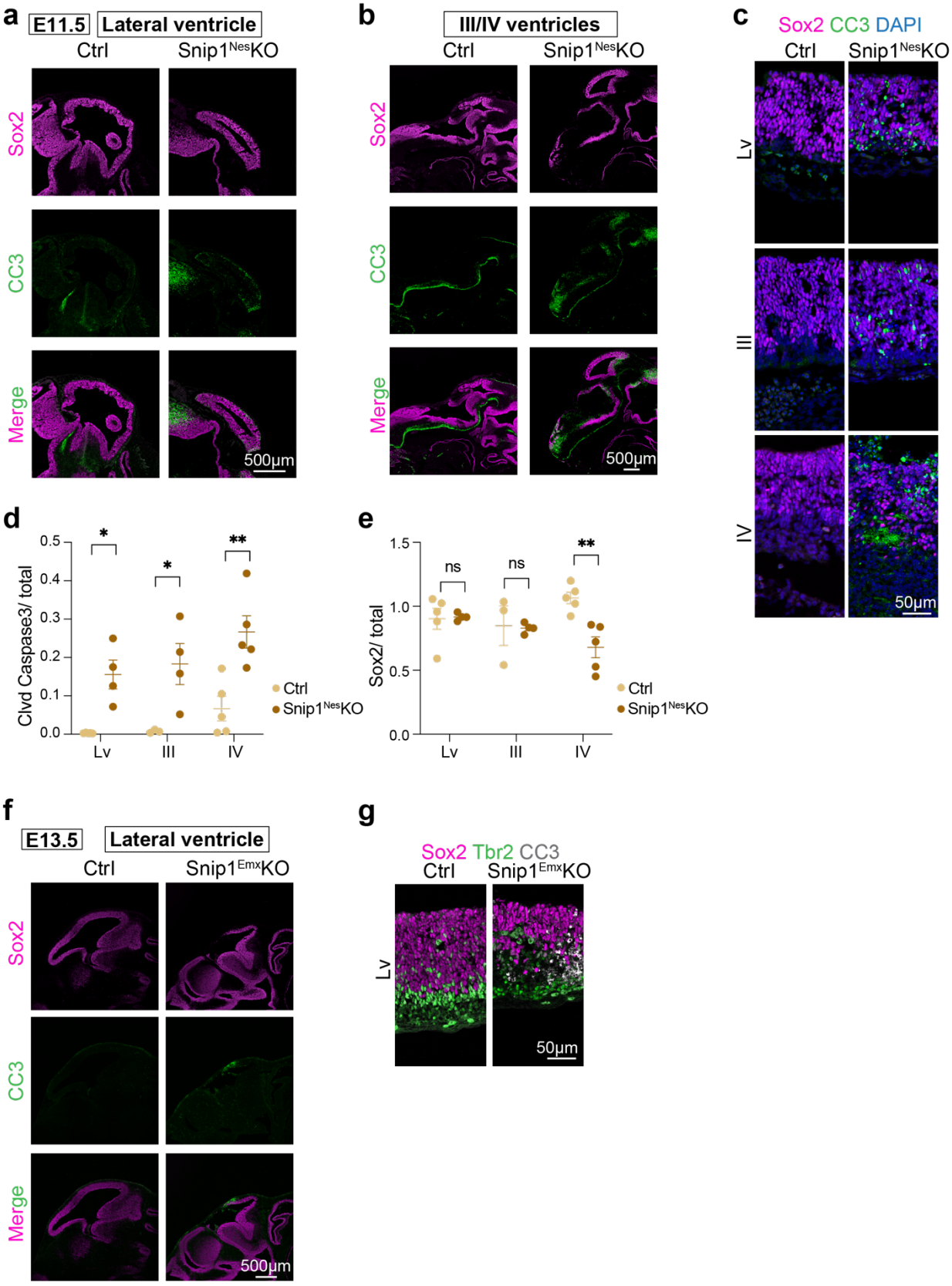
a
E11.5
Lateral ventricle
Ctrl
Snip1NesKO
Sox2
CC3
Merge
500μm
b
III/IV ventricles
Ctrl
Snip1NesKO
Sox2
CC3
Merge
500μm
c
Sox2 CC3 DAPI
Ctrl
Snip1NesKO
Lv
III
IV
50μm
d
Clvd Caspase3/ total
0.5
0.4
0.3
0.2
0.1
0.0
*
*
**
Lv
III
IV
Ctrl
Snip1NesKO
e
Sox2/ total
1.5
1.0
0.5
0.0
ns
ns
**
Lv
III
IV
Ctrl
Snip1NesKO
f
E13.5
Lateral ventricle
Ctrl
Snip1EmxKO
Sox2
CC3
Merge
500μm
g
Sox2 Tbr2 CC3
Ctrl
Snip1EmxKO
Lv
50μm

Fig. 2 Induction of apoptosis occurs in the *Snip1*^{Nes}-KO brains as early as E11.5.

a-b IF of Sox2 and CC3 in sagittal cryosections of the E11.5 brain. Germinal zones around lateral ventricle (Lv, forebrain) (**a**) and 3rd (midbrain) /4th (hindbrain) ventricles (**b**) were examined. Bar, 500 μm.

c IF with a higher magnification staining against Sox2, CC3, and DAPI of the E11.5 brain. Bar, 50 μm.

d-e Quantification of CC 3-positive and Sox2-positive cells in the neuroepithelial lining of the ventricles of control and *Snip1*^{Nes}-KO embryos at E11.5. DAPI staining was used to count the total number of cells. Each data point represents one image. Data are presented as mean ± SEM, and two-way ANOVA was used for statistical analysis. ns = not statistically significant; *p <0.05; **p <0.01.

f IF of Sox2 and CC3 in sagittal cryosections of control and *Snip1*^{Nes}-KO brains at E13.5. Germinal zones around lateral ventricle (**f**) and 3rd /4th ventricles (**g**) were examined. Bar, 500 μm.

g IF of Sox2 and CC3 overlayed with an intermediate progenitor marker Tbr2 in the control and *Snip1*^{Emx}-KO brains at E13.5. Bar, 50 μm.

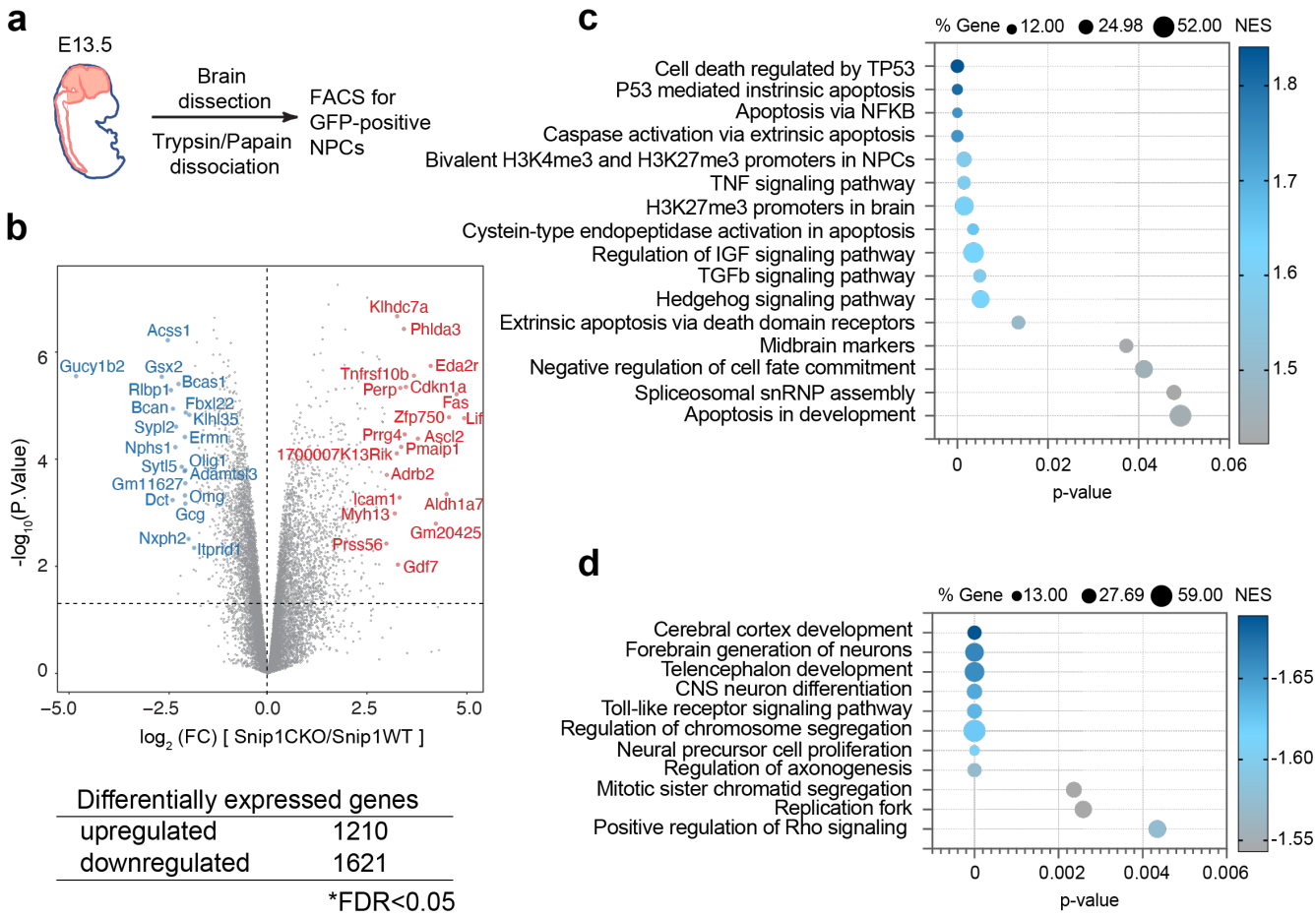
a
E13.5
Brain dissection
Trypsin/Papain dissociation
FACS for GFP-positive NPCs
b
Acss1
Gucy1b2
Gsx2
Bcas1
Rlbp1
Bcan
Fbxl22
Klhl35
Sypl2
Ermn
Nphs1
Sytl5
Olig1
Adamtsl3
Gm11627
Dct
Omg
Gcg
Nxph2
Itprid1
Klhdc7a
Phlda3
Eda2r
Tnfrsf10b
Perp
Cdkn1a
Fas
Zfp750
Lif
Prrg4
Ascl2
1700007K13Rik
Pmaip1
Adrb2
Icam1
Aldh1a7
Myh13
Gm20425
Prss56
Gdf7
-log10(P.Value)
log2 (FC) [Snip1CKO/Snip1WT]
Differentially expressed genes
upregulated 1210
downregulated 1621
*FDR<0.05
c
% Gene 12.00 24.98 52.00 NES
Cell death regulated by TP53
P53 mediated instrinsic apoptosis
Apoptosis via NFKB
Caspase activation via extrinsic apoptosis
Bivalent H3K4me3 and H3K27me3 promoters in NPCs
TNF signaling pathway
H3K27me3 promoters in brain
Cystein-type endopeptidase activation in apoptosis
Regulation of IGF signaling pathway
TGFb signaling pathway
Hedgehog signaling pathway
Extrinsic apoptosis via death domain receptors
Midbrain markers
Negative regulation of cell fate commitment
Spliceosomal snRNP assembly
Apoptosis in development
p-value
d
% Gene 13.00 27.69 59.00 NES
Cerebral cortex development
Forebrain generation of neurons
Telencephalon development
CNS neuron differentiation
Toll-like receptor signaling pathway
Regulation of chromosome segregation
Neural precursor cell proliferation
Regulation of axonogenesis
Mitotic sister chromatid segregation
Replication fork
Positive regulation of Rho signaling
p-value

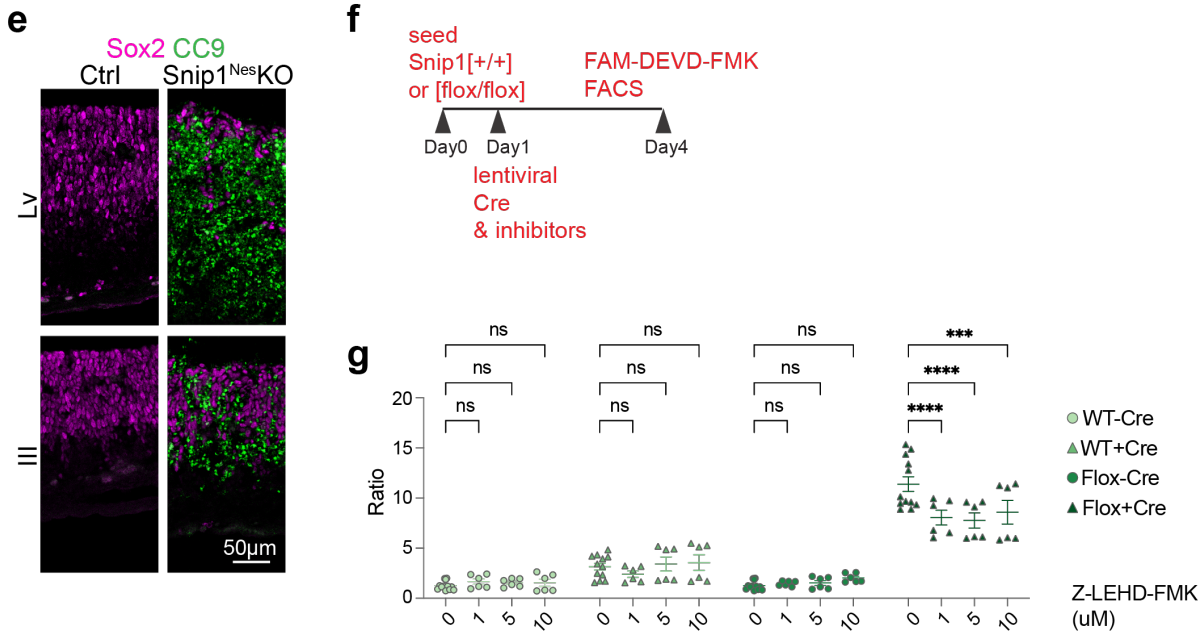
e
Sox2 CC9
Ctrl
Snip1NesKO
Lv
III
50μm
f
seed
Snip1[+/+]
or [flox/flox]
FAM-DEVD-FMK
FACS
Day0
Day1
Day4
lentiviral
Cre
& inhibitors
g
Ratio
ns
***
****
WT-Cre
WT+Cre
Flox-Cre
Flox+Cre
Z-LEHD-FMK
(uM)

Fig. 3 Snip1 suppresses genes involved in apoptosis and signal transduction and promotes genes for brain development.

a Schematic of the brain NPC collection.

b Volcano plot and the number of differentially expressed genes between the control and *Snip1*^{Nes}-KO NPCs. The table shows the number of genes that passed the cutoff of FDR <0.05. FDR was calculated by the Benjamini & Hochberg method.

c-d Bubble plots of the enriched gene sets in upregulated genes (**c**) and downregulated genes (**d**) in *Snip1*^{Nes}-KO vs. control NPCs. Differentially expressed genes were first ranked by their fold change, p-value, and expression level before Gene Set Enrichment Analysis (GSEA) was performed. P-values were calculated by one-tailed Kolmogorov–Smirnov test.

e IF of cleaved caspase 9 (CC9) overlayed with Sox2 and Tuj1 in sagittal cryosections of the E13.5 brain. Bar, 50 μm.

f Schematic of transduction with mCherry-Cre lentivirus and treatment with inhibitors in Snip1[+/+] and Snip1[flox/flox] NPCs.

g The percentage of cells with active caspase 3 quantified by FACS. Caspase 9 inhibitor (Z-LEHD-FMK) was added along with mCherry-Cre lentivirus.

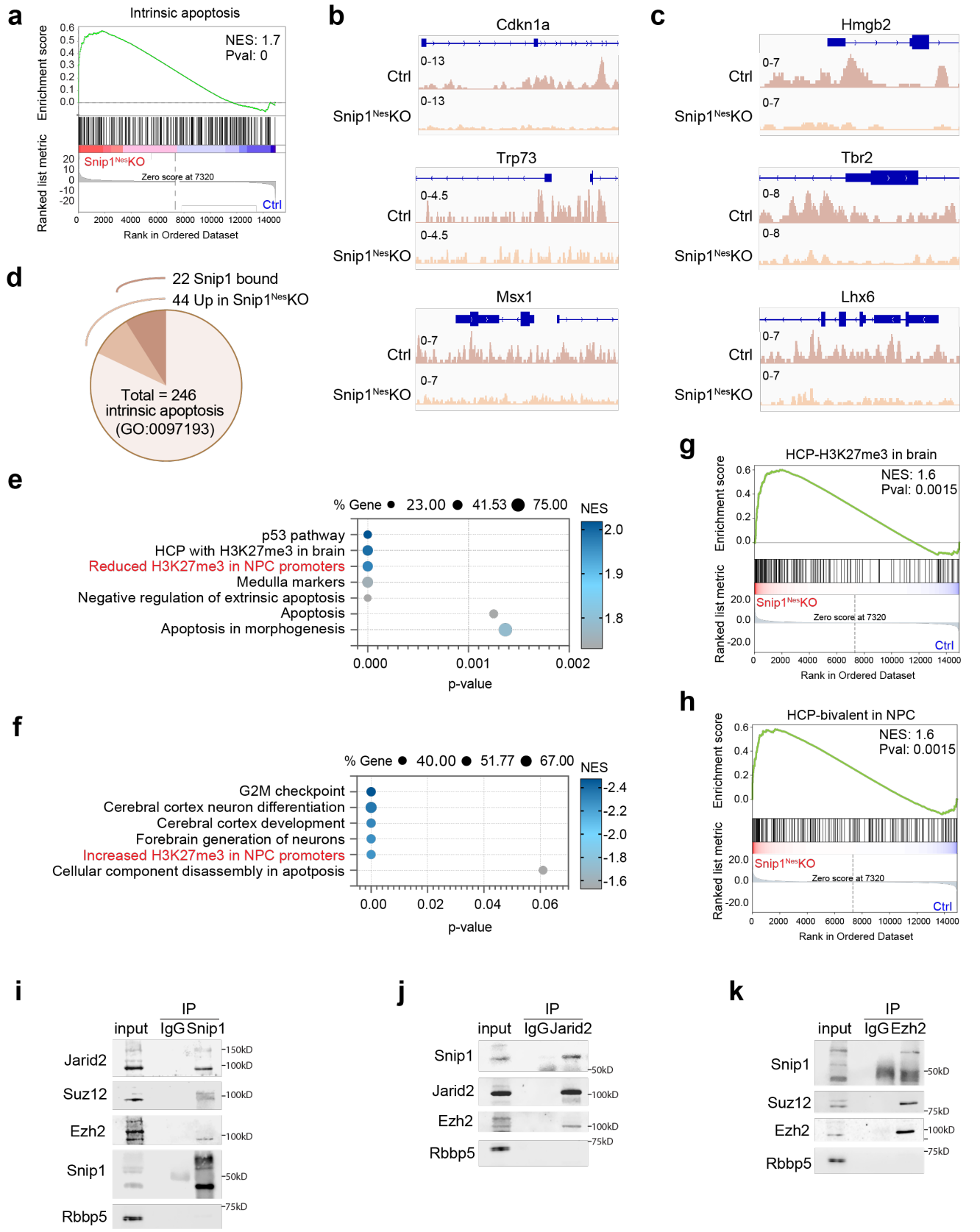
a
Intrinsic apoptosis
NES: 1.7
Pval: 0
Enrichment score
Ranked list metric
Snip1NesKO
Zero score at 7320
Ctrl
Rank in Ordered Dataset
b
Cdkn1a
Trp73
Msx1
Ctrl
Snip1NesKO
c
Hmgb2
Tbr2
Lhx6
d
22 Snip1 bound
44 Up in Snip1NesKO
Total = 246
intrinsic apoptosis
(GO:0097193)
e
% Gene
23.00
41.53
75.00
NES
p53 pathway
HCP with H3K27me3 in brain
Reduced H3K27me3 in NPC promoters
Medulla markers
Negative regulation of extrinsic apoptosis
Apoptosis
Apoptosis in morphogenesis
p-value
f
% Gene
40.00
51.77
67.00
G2M checkpoint
Cerebral cortex neuron differentiation
Cerebral cortex development
Forebrain generation of neurons
Increased H3K27me3 in NPC promoters
Cellular component disassembly in apoptosis
g
HCP-H3K27me3 in brain
NES: 1.6
Pval: 0.0015
h
HCP-bivalent in NPC
NES: 1.6
Pval: 0.0015
i
input
IP
IgG
Snip1
Jarid2
Suz12
Ezh2
Rbbp5
j
Jarid2
k
Ezh2

Fig. 4 Snip1 binds to chromatin to regulate gene expression in NPCs.

a Representative GSEA of upregulated genes in *Snip1*^{Nes}-KO NPCs. Upregulated genes were enriched in gene categories involving intrinsic apoptosis. Differentially expressed genes were first ranked by their fold change and p-value before GSEA was performed. P-values were calculated by one-tailed Kolmogorov–Smirnov test.

b-c Snip1 CUT&RUN tracks visualized by Integrative Genomics Viewer (IGV) at (**b**) upregulated genes and (**c**) downregulated genes.

d Pie chart showing the proportions of intrinsic apoptosis-related genes that are upregulated in *Snip1*^{Nes}-KO NPCs and/or bound by Snip1.

e-f Bubble plots listing the enriched gene sets in Snip1-bound genes that became (**e**) upregulated genes and (**f**) downregulated genes in *Snip1*^{Nes}-KO NPCs vs. control NPCs.

g-h Representatives of GSEA of upregulated genes in *Snip1*^{Nes}-KO NPCs. Upregulated genes were enriched in (**g**) high-CpG-density promoters with H3K27me3 in the embryonic murine brain and (**h**) high-CpG-density promoters with bivalent (H3K27me3 and H3K4me3) marks in mouse NPCs. Differentially expressed genes were first ranked by their fold change and p-value before GSEA was performed. P-values were calculated by one-tailed Kolmogorov–Smirnov test.

i-k Co-immunoprecipitation followed by WB to examine the interaction between Snip1 and PRC2. (**i**) Snip1, (**j**) Jarid2, or (**k**) Ezh2 was immunoprecipitated in the NPC nuclear extract. Rbbp5 was a negative control.

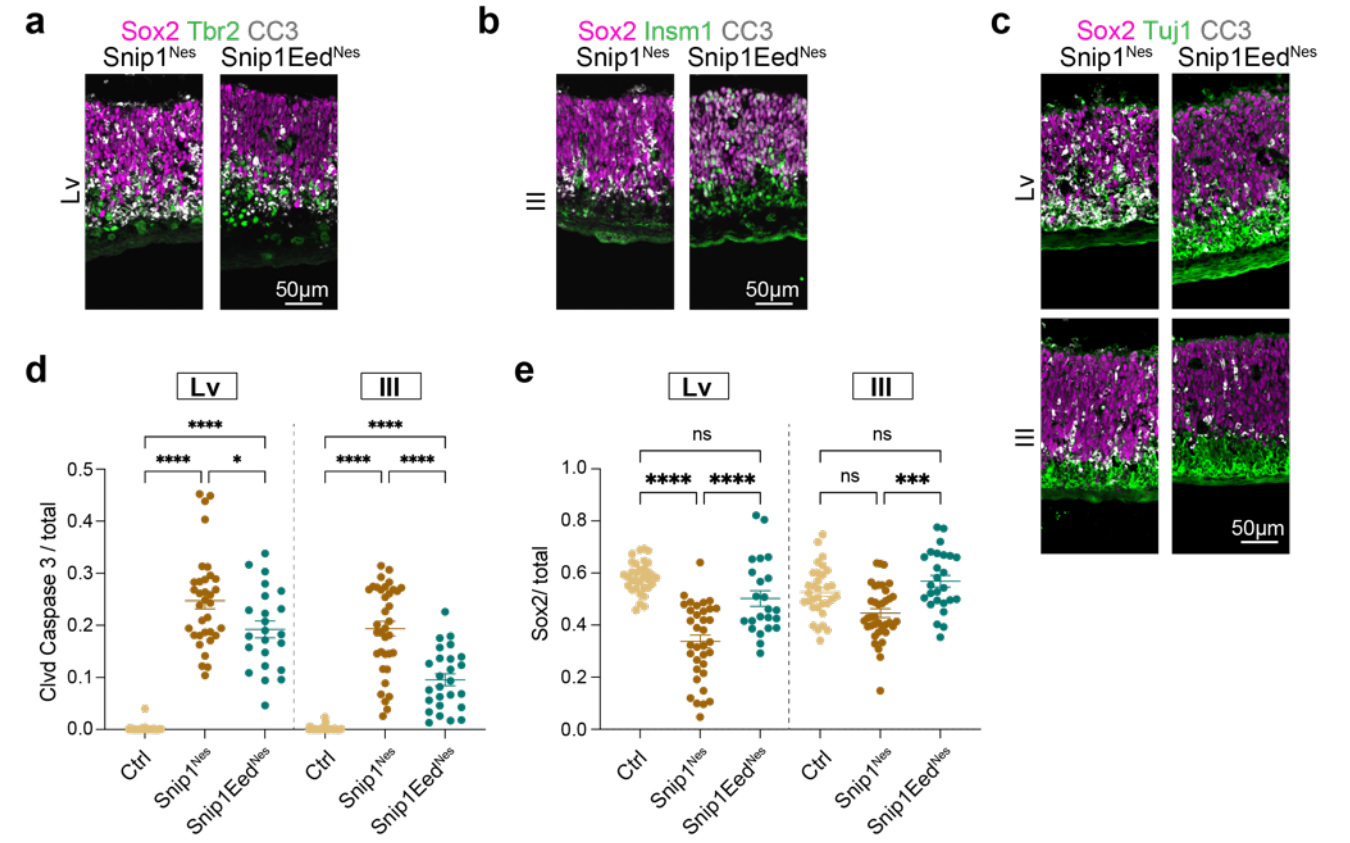

Fig. 5 Eed depletion reduces apoptosis in *Snip1*^{Nes}-KO NPCs, suggesting that PRC2–Snip1 interaction regulates apoptosis in the developing brain.

a-c IF of Sox2 and CC3 overlayed with neural lineage markers(**a**) Tuj1, (**b**) Tbr2, or (**c**) Insm1 of the E13.5 brain. Bar, 50 μm.

d-e Quantification of CC3 -positive (**d**) and Sox2-positive (**c**) cells in the neuroepithelial lining of lateral and third ventricles at E13.5. DAPI staining was used to count the total number of cells. Each data point represents one image (n=8 embryos for control, n=7 for *Snip1*^{Nes}-KO, n=5 for *Snip1*^{Nes}-*Eed*^{Nes}-dKO). Data are presented as mean ± SEM and two-way ANOVA was used for statistical analysis. ns = not statistically significant; *p<0.05; ***p <0.001; ****p <0.0001.

SUPPLEMENTAL DATA

Matsui_Supplementary Figure 1

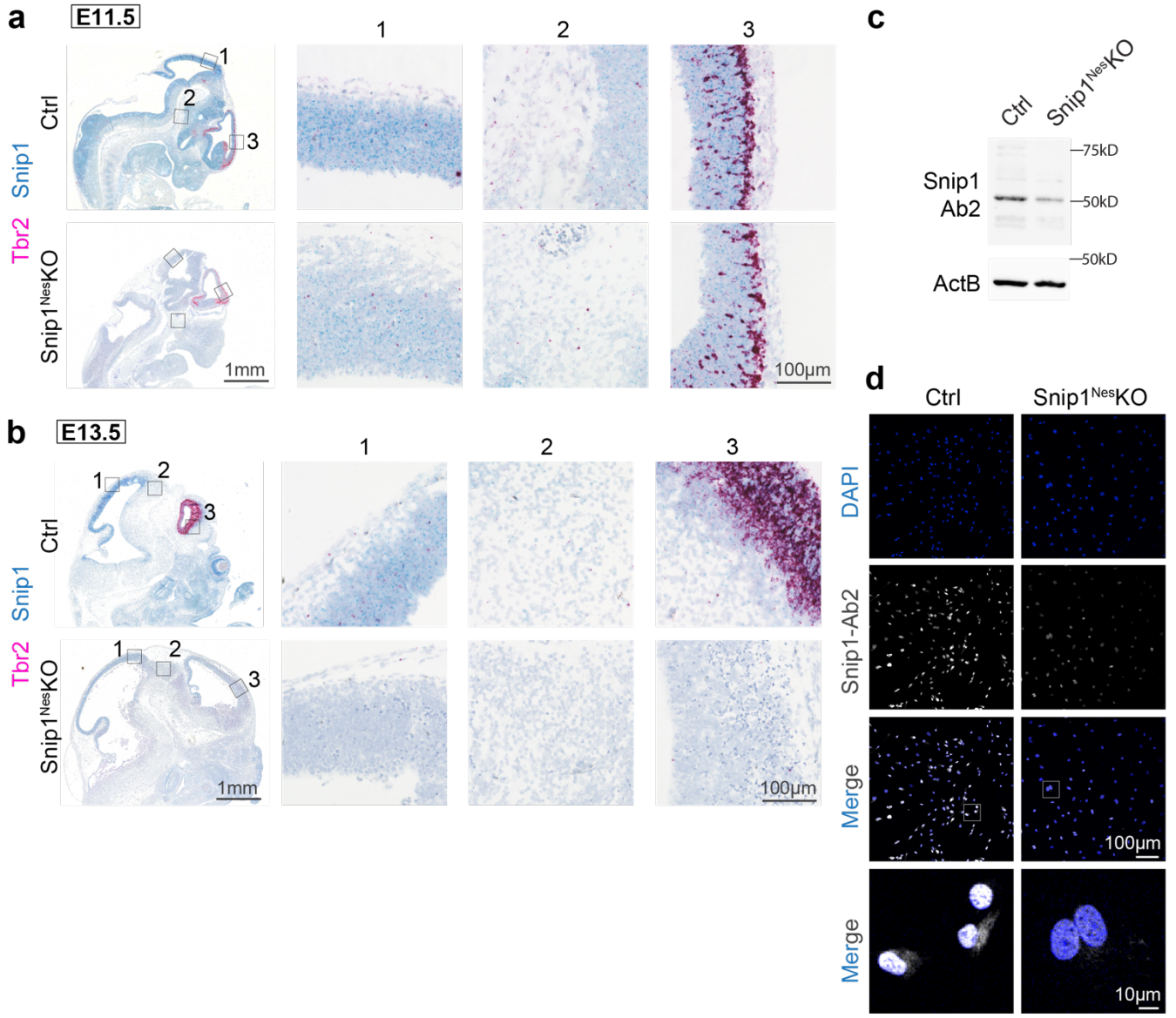

Supplemental Fig. 1 *Snip1* transcript is detected throughout the developing brain with strong expression in the neuroepithelia.

a-b RNAscope *in situ* hybridization of control and *Snip1*^{Nes}-KO cryosections at E11.5 (**a**) and E13.5 (**b**). Three magnified representative regions are shown (**1-3**). At E13.5, robust Snip1 expression (in teal) was detected in the neuroepithelia of the control embryo, whereas it is reduced in the *Snip1*^{Nes}-KO embryo., Cells positive for the intermediate progenitor marker Tbr2 (in red) were reduced in the *Snip1*^{Nes}-KO embryo. Bar, 1 mm (entire brain view) and 100 μm (magnified view).

c WB of control and *Snip1*^{Nes}-KO brains at E13.5. Snip1-Ab2; anti-Snip1 antibody from Thermo Fisher. **d** IF of Snip1 (Ab2; ThermoFisher antibody) and DAPI in control and *Snip1*^{Nes}-KO cultured NPCs. Bar, 100 μm (entire view) and 10 μm (magnified view).

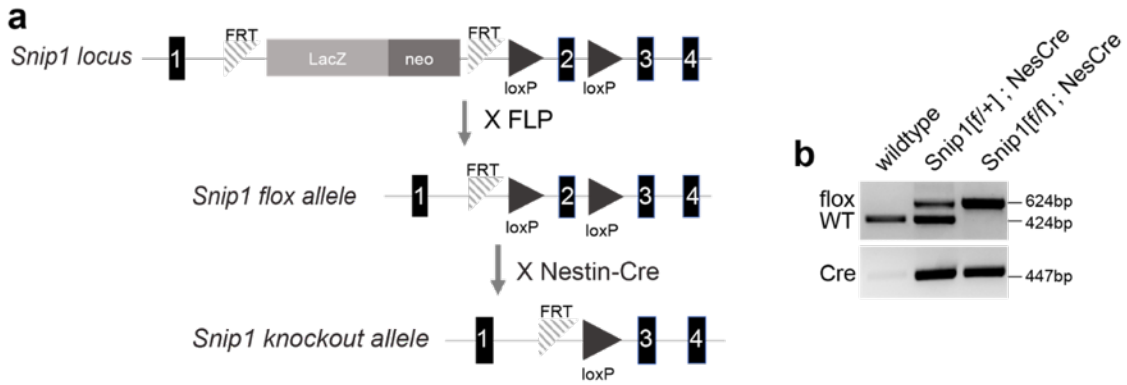

c

E13.5

Genotype	Exp.	Obs.	X^2	p-value
Snip1[+/+]; NesCre	9.5	12	-	-
Snip1[f/+]; NesCre	19	14	1.92	0.17
Snip1[f/f]; NesCre	9.5	12	0	>0.99
Total	38	38	2.63	0.27

d

weaning

Genotype	Exp.	Obs.	X^2	p-value
Snip1[+/+]; NesCre	15	38	-	-
Snip1[f/+]; NesCre	30	22	4.27	0.039*
Snip1[f/f]; NesCre	15	0	38	<0.0001****
Total	60	60	52.4	<0.0001****

Supplemental Fig. 2 Mice with Snip1-depleted neural progenitor cells are not viable by weaning age.
a Schematic representation of *Snip1* locus containing the LacZ cassette and loxP sites flanking exon 2. Excision of the LacZ cassette by flippase (FLP) generates *Snip1*[flox] allele. Subsequent excision of exon 2 by Cre recombinase driven by *Nestin* promoter (Nestin:Cre) generates *Snip1* knockout allele.
b Genotyping PCR of wildtype allele, *Snip1*[flox] allele, and allele with Cre recombinase transgene.
c-d Viability of Snip1[+/+]^{Nes}, Snip1[flox/+]^{Nes} and Snip1[flox/flox]^{Nes} mice at E13.5 (**c**) and at the weaning age (between 3 and 4 weeks after birth, **d**). Chi-square test was performed to determine if the mice of three genotypes are viable at the Mendelian ratio. *p<0.05 and ****p <0.0001. *Snip1*^{Nes}-KO embryos were obtained at the expected Mendelian frequency at E13.5; however, no *Snip1*^{Nes}-KO mice were obtained at the weaning age.

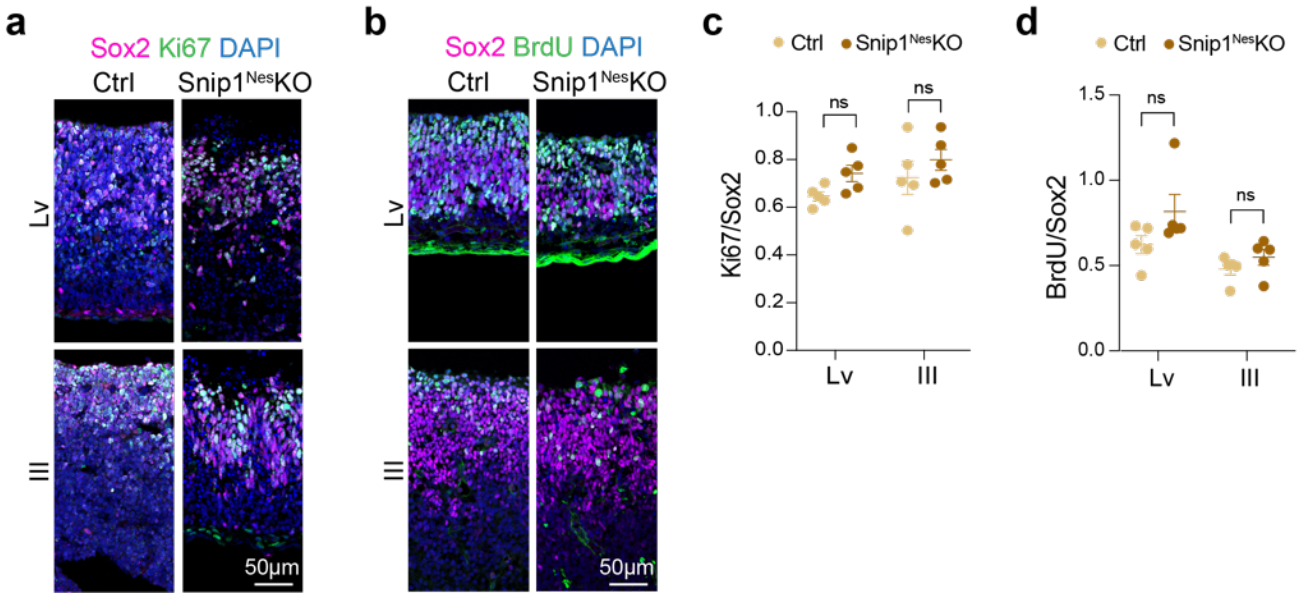

Supplemental Fig. 3 Snip1 is dispensable for the proliferation of NPCs *in vivo*.

a-b IF of Sox2 and Ki67 (**a**, n=3 sibling pairs) and BrdU (**b**, n=1 sibling pair) in DAPI-stained sagittal cryosections of the E13.5 brain. Germinal zones around the lateral ventricle (forebrain), 3rd ventricle (midbrain) and 4th ventricle (hindbrain) were examined. Bar, 50 μm.

c-d Quantification of the proliferating NPC population in control and *Snip1*^{Nes}-KO embryos at E13.5. Each data point represents one image. Data are presented as mean ± SEM and two-way ANOVA was used for statistical analysis. ns = not statistically significant; **p <0.01.

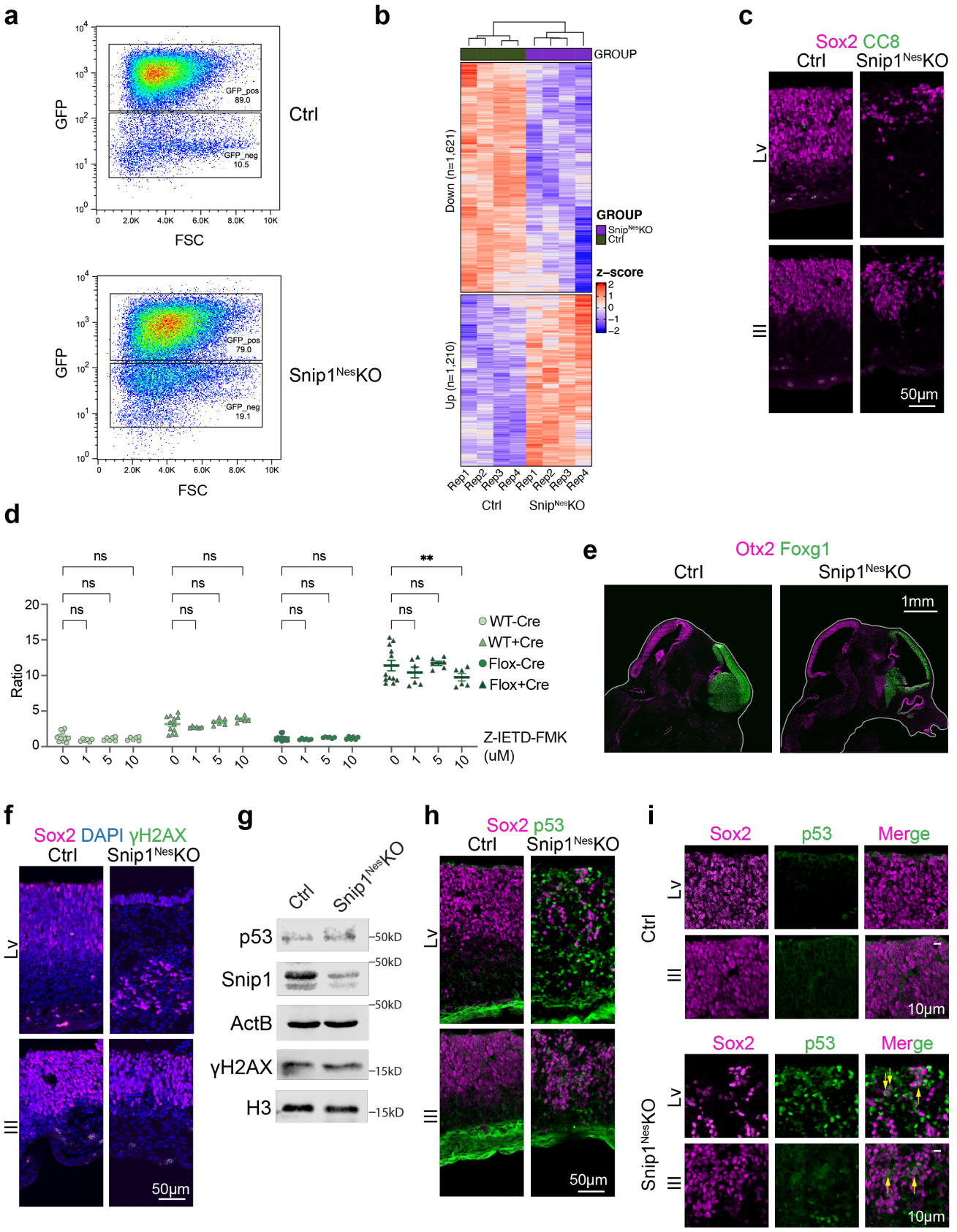
a
GFP
FSC
GFP_pos 89.0
GFP_neg 10.5
Ctrl
GFP_pos 79.0
GFP_neg 19.1
Snip1NesKO
b
GROUP
Down (n=1,621)
Up (n=1,210)
GROUP
SnipNesKO
Ctrl
z-score
Rep1 Rep2 Rep3 Rep4 Rep1 Rep2 Rep3 Rep4
Ctrl SnipNesKO
c
Sox2 CC8
Ctrl Snip1NesKO
Lv
III
50μm
d
Ratio
ns
**
WT-Cre
WT+Cre
Flox-Cre
Flox+Cre
Z-IETD-FMK (uM)
e
Otx2 Foxg1
Ctrl Snip1NesKO
1mm
f
Sox2 DAPI γH2AX
Ctrl Snip1NesKO
Lv
III
50μm
g
Ctrl Snip1NesKO
p53
Snip1
ActB
γH2AX
H3
50kD
15kD
h
Sox2 p53
Ctrl Snip1NesKO
Lv
III
50μm
i
Sox2 p53 Merge
Ctrl
Snip1NesKO
Lv
III
10μm

Supplemental Fig. 4 *Snip1*^{Nes}-KO-induced cell death does not involve DNA damage response.

a FACS density plots of the control and *Snip1*^{Nes}-KO brain cells. The proportion of the GFP-positive population is reduced in the *Snip1*^{Nes}-KO brains vs. control brains.

b Heatmap of differentially expressed genes (by the criterion of FDR<0.05) in *Snip1*^{Nes}-KO and control NPCs.

c IF of cleaved caspase 8, Sox2, and Tuj1 in sagittal cryosections of E13.5 brains. Bar, 50 μm.

d Quantification of cells with active caspase 3 quantified by FACS. Snip1 was depleted in Snip1[flox/flox] NPCs by lentiviral mCherry-Cre in the presence or absence of the caspase 8 inhibitor, Z-IETD-FMK.

e IF of Foxg1 (a forebrain marker) and Otx2 (a mid/hindbrain marker) in the control and *Snip1*^{Nes}-KO brains at E13.5. Bar, 1 mm.

f IF of γH2AX and Sox2 in sagittal cryosections of E13.5 brains. Bar, 50 μm.

g WB detecting γH2AX and p53 in the nuclear extract of control and *Snip1*^{Nes}-KO brains at E13.5.

h-i IF of p53 and Sox2 in sagittal cryosections of E13.5 brains. Bar, (**h**) 50 μm and (**i**) 10 μm.

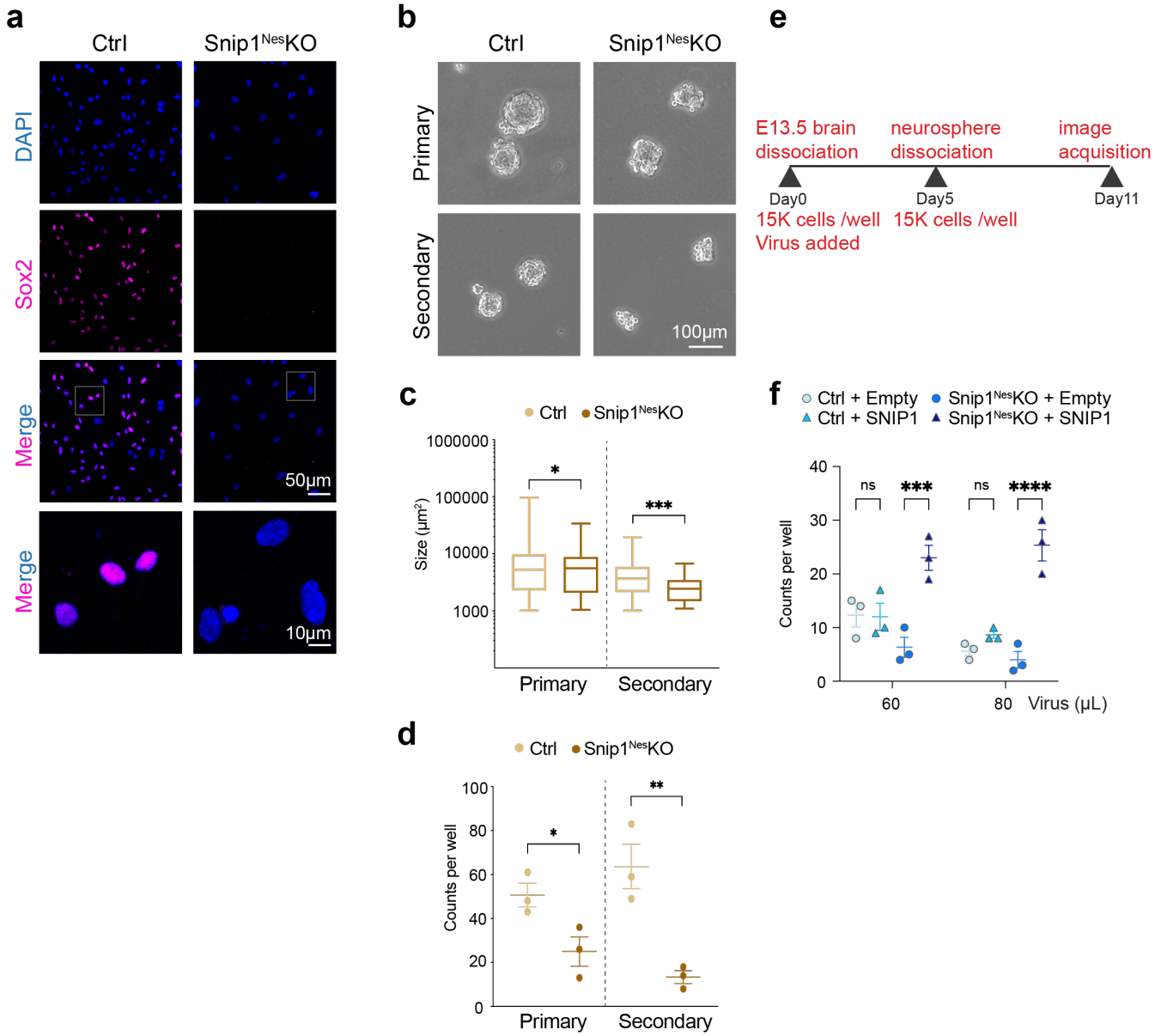

Supplemental Fig. 5 Snip1 is pivotal for the self-renewal property of NPCs in culture.

a IF of Sox2 and DAPI in control and *Snip1*^{Nes}-KO cultured NPCs. Bar, 50 μm (entire view) and 10 μm (magnified view).

b Brightfield images of the sequential neurosphere assay with control and *Snip1*^{Nes}-KO NPCs. For primary neurosphere formation, 10,000 cells were seeded to each well of low-attachment 6-well plates (Day 0). For secondary neurosphere formation, primary neurospheres were dissociated and 3,000 cells were seeded to each well. All neurospheres were imaged after 5 days of culture. Bar, 100 μm.

c-d Quantification of the neurosphere size and counts per well. Data are presented as a box plot (**c**) and mean ± SEM (**d**) and unpaired t-test was used for statistical analysis. *p<0.05; **p <0.01; ***p <0.001. Snip1-depleted NPCs cannot maintain their self-renewal property in culture.

e Schematic of a neurosphere rescue experiment.

f Quantification of the counts of neurospheres per well. Data are presented as mean ± SEM and two-way ANOVA was used for statistical analysis. ns = not statistically significant; ***p <0.001; ****p <0.0001. Overexpressing SNIP1 in *Snip1*^{Nes}-KO NPCs increased neurosphere formation.

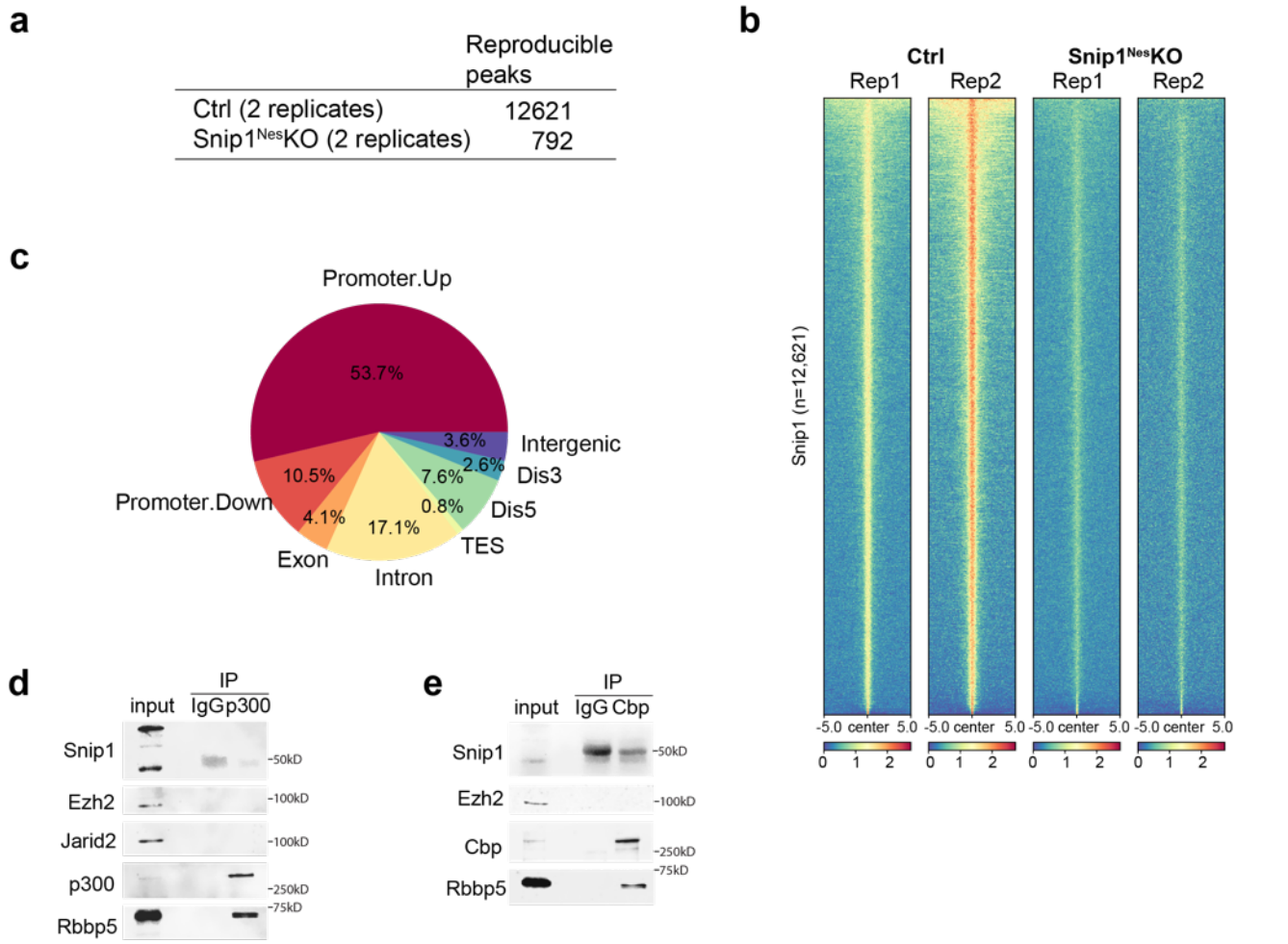

Supplemental Fig. 6 Most Snip1 proteins on chromatin bind to promoters.

a The number of reproducible peaks bound by Snip1 in the control and *Snip1*^{Nes}-KO NPCs. Peaks were called by SICER with the cutoff of FDR <0.05. FDR was calculated by using the Lima-Voom algorithm (Law et al., 2014) (see Methods).

b Heatmaps represent the binding intensity of 2 biological replicates of Snip1 CUT&RUN in control and *Snip1*^{Nes}-KO NPCs. Binding intensity for 5 kb on either side all 12,621 Snip1 CUT&RUN peaks are shown. Blue indicates low intensity and red indicates high intensity.

c Proportions of Snip1 binding to different genomic features. Over 60% of Snip1 binding was detected in promoter regions.

d-e Co-immunoprecipitation followed by WB to examine the interaction between Snip1 and p300/Cbp. (**d**) p300 or (**e**) Cbp was immunoprecipitated in the NPC nuclear extract. Anti-IgG antibody was used as the control for IP and Rbbp5 was a positive control for p300 and Cbp interactions.

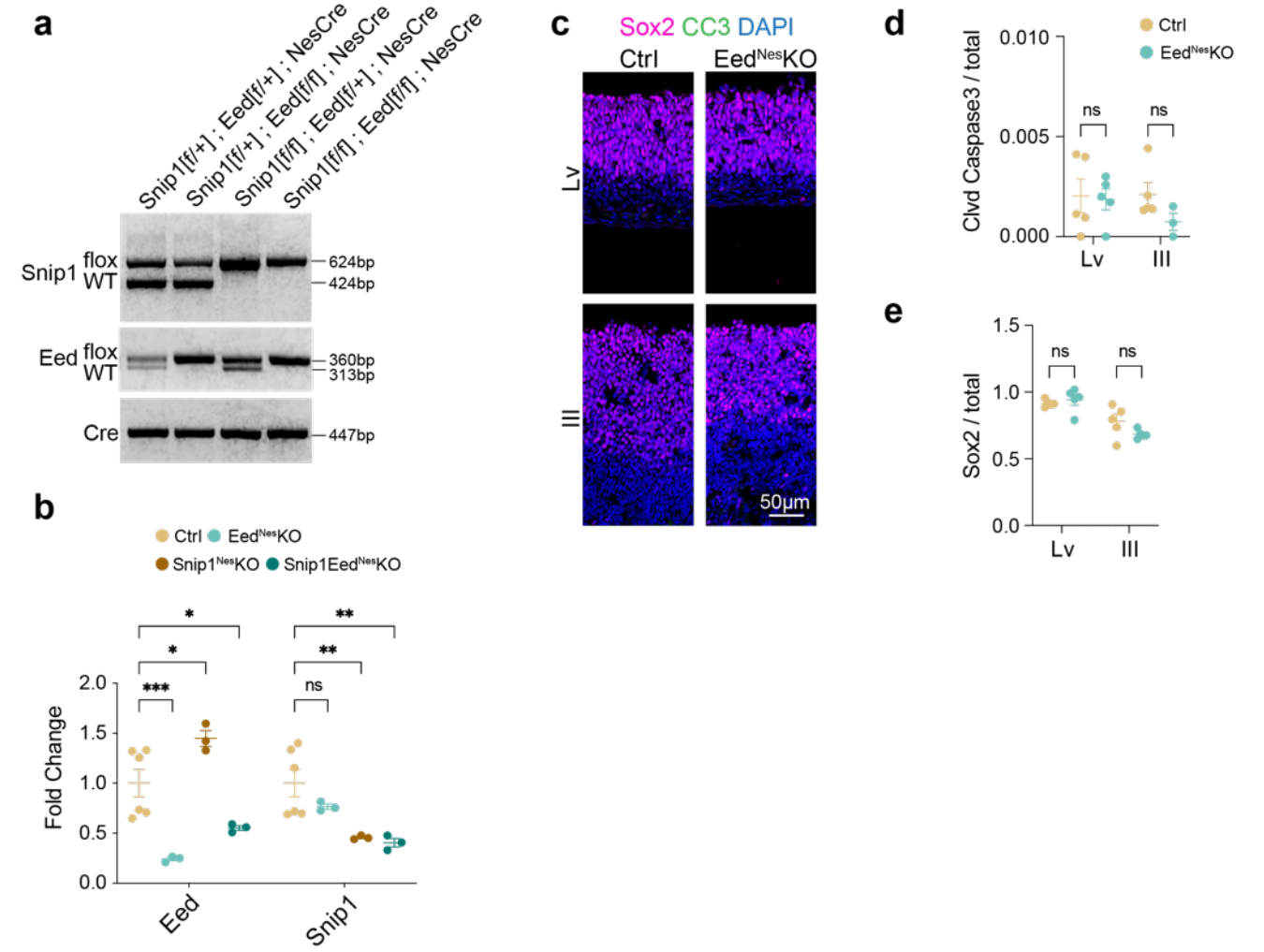

Supplemental Fig. 7 Characterization of *Eed*^{Nes}-KO and *Snip1*^{Nes}-*Eed*^{Nes}-dKO.

a Genotyping PCR of *Snip1*-flox allele, *Eed*-flox allele, and allele with Nes:Cre recombinase.

b Quantitative PCR of *Eed* and *Snip1* transcripts in the NPCs from E13.5 brains. The Cq values of each gene were normalized to that of a housekeeping gene *Gapdh*. The expression level of each gene is relative to the level in the control brain. Data are presented as mean ± SEM, and two-way ANOVA was used for statistical analysis. ns = not statistically significant; *p<0.05; **p <0.01; ***p <0.001.

c IF analysis of Sox2, CC3, and DAPI of the E13.5 brain. Bar, 50 μm.

d-e Quantification of CC3-positive and Sox2-positive cells in the neuroepithelia of the ventricles of control and *Eed*^{Nes}-KO embryos at E13.5. DAPI staining was used to quantify the total number of cells. Each data point represents one image. Data are presented as mean ± SEM, and two-way ANOVA was used for statistical analysis. ns = not statistically significant.

Supplemental Table 1. List of antibodies.

Target	Vendor	Catalog #	Assay (dilution)
Normal Rabbit IgG	RD Systems	AB-105-C	IP CUT&RUN
Normal Goat IgG	RD Systems	AB-108-C	IP CUT&RUN
Jarid2	Novus Biological	NB100-2214	IP WB (1:1000)
Ezh2	Active Motif	39934	WB (1:1000)
Ezh2	Active Motif	39076	IP WB (1:1000)
Suz12	Cell Signaling Technology	3737	WB (1:1000)
Suz12	Active Motif	39057	WB (1:1000)
Snip1	Thermo Fisher Scientific	29412	IP IF (1:50) WB (1:1000) CUT&RUN
Snip1	ProteinTech	14950-I-AP	IP IF (1:50) WB (1:1000)
Snip1	Abcam	ab19611	IF (1:50)
Rbbp5	Bethyl Laboratories	A300-109A	WB (1:1000)
p300	RD Systems	AF3789	IP WB (1:1000)
Cbp	GeneTex	GTX101249	IP WB (1:1000)
H3K27me3	Millipore	07-449	CUT&RUN
H3K27ac	Abcam	ab4729	CUT&RUN
β-Actin	Sigma-Aldrich	A1978	WB (1:2000)
Sox2	Santa Cruz Biotechnology	sc-17320	IF (1:150)
Tbr2	Thermo Fisher Scientific	14-4875-80	IF (1:200)

Cleaved caspase3 (Asp175)	Cell Signaling Technology	9661	IF (1:200)
Ki-67	Cell Signaling Technology	9129	IF (1:100)
Foxg1	Abcam	ab196868	IF (1:200)
Otx2	R&D Systems	AF1979	IF (1:150)
Ki-67-eFluor® 450	Thermo Fisher Scientific	48-5698-82	IF (1:50)
Map2	Abcam	ab5392	IF (1:5,000)

Supplemental Table 2. Genotype primers and conditions.

Line	Forward 5'->3'	Reverse 5'->3'	Anneal	Product Size (bp)
***Snip1*-tm1a**	GATGGAGCAGCATTGTAGGC	GAACTTCGGAATAGGAACTTCG	60 °C	234
***Snip1*-flox**	GATGGAGCAGCATTGTAGGC	CTTCTTGGCTGGGGACCTTT	60 °C	424(WT) 624(flox)
***Eed*-flox**	GGGACGTGCTGACATTTTCT	CTTGGGTGGTTTGGCTAAGA	52 °C	313(WT) ~360(flox)
***Ep300*-flox**	GTGAGTTGATGTCCCTGTCG	CAGACACCCTCTTGCACTCA	54 °C	247(WT) ~400(flox)
***Cbp*-flox**	CCTGGTTGCCTATGCTAAGAAAG	CTGCTCTACCTAAATTCCCAG	60 °C	~650(WT) ~800 (flox)
***alt. Cbp*-flox**	TGGGTGTGTAGATGCAAGGT	GGCTTGAACGCTGAAAGAAC	56 °C	171(WT) ~220(flox)
***Actin*-FLPe**	ACTCCGTTAGGCCCTTCATT	GCATCATGTGCTGCTGAACT	56 °C	874
***Nestin*-Cre**	ATGCCCAAGAAGAAGAGGAAGGT	GAAATCAGTGCGTTCGAACGCTAGA	56 °C	447
***Emx1*-Cre**	ATGCCCAAGAAGAAGAGGAAGGT	GAAATCAGTGCGTTCGAACGCTAGA	56 °C	447
***Sox2*-eGFP**	CGTAAACGGCCACAAGTTCA	CTCAGGTAGTGGTTGTCGGG	56 °C	543

Supplemental Table 3. Primers for RT-qPCR.

Gene	Forward 5'->3'	Reverse 5'->3'
Snip1	TCGGGAAGGAACTTTGAGGT	TCTTGGTCCGTGGTGACTTG
Alt. Snip1	CCGGTCCCCAGCCAAG	TCCTCACGTTCCTGCTTCAC
Eed	AAGTTGAGCAGCGACGAGAA	ATTTGGCGTATTTGTGGGCG
Gapdh	TCCCACTCTTCCACCTTCGATGC	GGGTCTGGGATGGAAATTGTGAGG

REFERENCE

Ammous, Z., Rawlins, L.E., Jones, H., Leslie, J.S., Wenger, O., Scott, E., Deline, J., Herr, T., Evans, R., Scheid, A.*, et al.* (2021). A biallelic SNIP1 Amish founder variant causes a recognizable neurodevelopmental disorder. PLoS Genet *17*, e1009803.

Arnold, K., Sarkar, A., Yram, M.A., Polo, J.M., Bronson, R., Sengupta, S., Seandel, M., Geijsen, N., and Hochedlinger, K. (2011). Sox2(+) adult stem and progenitor cells are important for tissue regeneration and survival of mice. Cell Stem Cell *9*, 317-329.

Bedner, E., Smolewski, P., Amstad, P., and Darzynkiewicz, Z. (2000). Activation of caspases measured in situ by binding of fluorochrome-labeled inhibitors of caspases (FLICA): correlation with DNA fragmentation. Exp Cell Res *259*, 308-313.

Bieberich, E., MacKinnon, S., Silva, J., and Yu, R.K. (2001). Regulation of apoptosis during neuronal differentiation by ceramide and b-series complex gangliosides. J Biol Chem *276*, 44396-44404.

Blaschke, A.J., Staley, K., and Chun, J. (1996). Widespread programmed cell death in proliferative and postmitotic regions of the fetal cerebral cortex. Development *122*, 1165-1174.

Boldin, M.P., Goncharov, T.M., Goltsev, Y.V., and Wallach, D. (1996). Involvement of MACH, a novel MORT1/FADD-interacting protease, in Fas/APO-1- and TNF receptor-induced cell death. Cell *85*, 803-815.

Bronstein, R., Kyle, J., Abraham, A.B., and Tsirka, S.E. (2017). Neurogenic to Gliogenic Fate Transition Perturbed by Loss of HMGB2. Front Mol Neurosci *10*, 153.

Chang, L., An, Z., Zhang, J., Zhou, F., Wang, D., Liu, J., and Zhang, Y. (2021). H3K27 demethylase KDM6B aggravates ischemic brain injury through demethylation of IRF4 and Notch2-dependent SOX9 activation. Mol Ther Nucleic Acids *24*, 622-633.

Chen, E.Y., Tan, C.M., Kou, Y., Duan, Q., Wang, Z., Meirelles, G.V., Clark, N.R., and Ma'ayan, A. (2013). Enrichr: interactive and collaborative HTML5 gene list enrichment analysis tool. BMC Bioinformatics *14*, 128.

Dobin, A., and Gingeras, T.R. (2015). Mapping RNA-seq Reads with STAR. Curr Protoc Bioinformatics *51*, 11 14 11-11 14 19.

Evans, M.K., Matsui, Y., Xu, B., Willis, C., Loome, J., Milburn, L., Fan, Y., Pagala, V., and Peng, J.C. (2020). Ybx1 fine-tunes PRC2 activities to control embryonic brain development. Nat Commun *11*, 4060.

Faust, C., Lawson, K.A., Schork, N.J., Thiel, B., and Magnuson, T. (1998). The Polycomb-group gene eed is required for normal morphogenetic movements during gastrulation in the mouse embryo. Development *125*, 4495-4506.

Faust, C., Schumacher, A., Holdener, B., and Magnuson, T. (1995). The eed mutation disrupts anterior mesoderm production in mice. Development *121*, 273-285.

Feng, X.H., Zhang, Y., Wu, R.Y., and Derynck, R. (1998). The tumor suppressor Smad4/DPC4 and transcriptional adaptor CBP/p300 are coactivators for smad3 in TGF-beta-induced transcriptional activation. Genes Dev *12*, 2153-2163.

Fernandez, J.P., Moreno-Mateos, M.A., Gohr, A., Miao, L., Chan, S.H., Irimia, M., and Giraldez, A.J. (2018). RES complex is associated with intron definition and required for zebrafish early embryogenesis. PLoS Genet *14*, e1007473.

Fujii, M., Lyakh, L.A., Bracken, C.P., Fukuoka, J., Hayakawa, M., Tsukiyama, T., Soll, S.J., Harris, M., Rocha, S., Roche, K.C.*, et al.* (2006). SNIP1 is a candidate modifier of the transcriptional activity of c-Myc on E box-dependent target genes. Mol Cell *24*, 771-783.

Gerritsen, M.E., Williams, A.J., Neish, A.S., Moore, S., Shi, Y., and Collins, T. (1997). CREB-binding protein/p300 are transcriptional coactivators of p65. Proc Natl Acad Sci U S A *94*, 2927-2932.

Gorski, J.A., Talley, T., Qiu, M., Puelles, L., Rubenstein, J.L., and Jones, K.R. (2002). Cortical excitatory neurons and glia, but not GABAergic neurons, are produced in the Emx1-expressing lineage. J Neurosci *22*, 6309-6314.

Hakem, R., Hakem, A., Duncan, G.S., Henderson, J.T., Woo, M., Soengas, M.S., Elia, A., de la Pompa, J.L., Kagi, D., Khoo, W.*, et al.* (1998). Differential requirement for caspase 9 in apoptotic pathways in vivo. Cell *94*, 339-352.
Holoch, D., and Margueron, R. (2017). Mechanisms Regulating PRC2 Recruitment and Enzymatic Activity. Trends Biochem Sci *42*, 531-542.
Janknecht, R., Wells, N.J., and Hunter, T. (1998). TGF-beta-stimulated cooperation of smad proteins with the coactivators CBP/p300. Genes Dev *12*, 2114-2119.
Kang-Decker, N., Tong, C., Boussouar, F., Baker, D.J., Xu, W., Leontovich, A.A., Taylor, W.R., Brindle, P.K., and van Deursen, J.M. (2004). Loss of CBP causes T cell lymphomagenesis in synergy with p27Kip1 insufficiency. Cancer Cell *5*, 177-189.
Kasper, L.H., Fukuyama, T., Biesen, M.A., Boussouar, F., Tong, C., de Pauw, A., Murray, P.J., van Deursen, J.M., and Brindle, P.K. (2006). Conditional knockout mice reveal distinct functions for the global transcriptional coactivators CBP and p300 in T-cell development. Mol Cell Biol *26*, 789-809.
Kim, R.H., Flanders, K.C., Birkey Reffey, S., Anderson, L.A., Duckett, C.S., Perkins, N.D., and Roberts, A.B. (2001). SNIP1 inhibits NF-kappa B signaling by competing for its binding to the C/H1 domain of CBP/p300 transcriptional co-activators. J Biol Chem *276*, 46297-46304.
Kim, R.H., Wang, D., Tsang, M., Martin, J., Huff, C., de Caestecker, M.P., Parks, W.T., Meng, X., Lechleider, R.J., Wang, T.*, et al.* (2000). A novel smad nuclear interacting protein, SNIP1, suppresses p300-dependent TGF-beta signal transduction. Genes Dev *14*, 1605-1616.
Kuida, K., Haydar, T.F., Kuan, C.Y., Gu, Y., Taya, C., Karasuyama, H., Su, M.S., Rakic, P., and Flavell, R.A. (1998). Reduced apoptosis and cytochrome c-mediated caspase activation in mice lacking caspase 9. Cell *94*, 325-337.
Kuida, K., Zheng, T.S., Na, S., Kuan, C., Yang, D., Karasuyama, H., Rakic, P., and Flavell, R.A. (1996). Decreased apoptosis in the brain and premature lethality in CPP32-deficient mice. Nature *384*, 368-372.
Kuleshov, M.V., Jones, M.R., Rouillard, A.D., Fernandez, N.F., Duan, Q., Wang, Z., Koplev, S., Jenkins, S.L., Jagodnik, K.M., Lachmann, A.*, et al.* (2016). Enrichr: a comprehensive gene set enrichment analysis web server 2016 update. Nucleic Acids Res *44*, W90-97.
Laugesen, A., Hojfeldt, J.W., and Helin, K. (2019). Molecular Mechanisms Directing PRC2 Recruitment and H3K27 Methylation. Mol Cell *74*, 8-18.
Law, C.W., Chen, Y., Shi, W., and Smyth, G.K. (2014). voom: Precision weights unlock linear model analysis tools for RNA-seq read counts. Genome Biol *15*, R29.
Lee, Y., Katyal, S., Downing, S.M., Zhao, J., Russell, H.R., and McKinnon, P.J. (2012). Neurogenesis requires TopBP1 to prevent catastrophic replicative DNA damage in early progenitors. Nat Neurosci *15*, 819-826.
Li, B., and Dewey, C.N. (2011). RSEM: accurate transcript quantification from RNA-Seq data with or without a reference genome. BMC Bioinformatics *12*, 323.
Li, J., Hart, R.P., Mallimo, E.M., Swerdel, M.R., Kusnecov, A.W., and Herrup, K. (2013). EZH2-mediated H3K27 trimethylation mediates neurodegeneration in ataxia-telangiectasia. Nat Neurosci *16*, 1745-1753.
Li, P., Nijhawan, D., Budihardjo, I., Srinivasula, S.M., Ahmad, M., Alnemri, E.S., and Wang, X. (1997). Cytochrome c and dATP-dependent formation of Apaf-1/caspase-9 complex initiates an apoptotic protease cascade. Cell *91*, 479-489.
Liberzon, A., Birger, C., Thorvaldsdottir, H., Ghandi, M., Mesirov, J.P., and Tamayo, P. (2015). The Molecular Signatures Database (MSigDB) hallmark gene set collection. Cell Syst *1*, 417-425.
Liu, X.Z., Zhang, Q., Jiang, Q., Bai, B.L., Du, X.J., Wang, F., Wu, L.H., Lu, X.L., Bao, Y.H., Li, H.L.*, et al.* (2018). Genetic screening and functional analysis of CASP9 mutations in a Chinese cohort with neural tube defects. CNS Neurosci Ther *24*, 394-403.
Meissner, A., Mikkelsen, T.S., Gu, H., Wernig, M., Hanna, J., Sivachenko, A., Zhang, X., Bernstein, B.E., Nusbaum, C., Jaffe, D.B.*, et al.* (2008). Genome-scale DNA methylation maps of pluripotent and differentiated cells. Nature *454*, 766-770.

Mikkelsen, T.S., Ku, M., Jaffe, D.B., Issac, B., Lieberman, E., Giannoukos, G., Alvarez, P., Brockman, W., Kim, T.K., Koche, R.P.*, et al.* (2007). Genome-wide maps of chromatin state in pluripotent and lineage-committed cells. Nature *448*, 553-560.
Muzio, M., Chinnaiyan, A.M., Kischkel, F.C., O'Rourke, K., Shevchenko, A., Ni, J., Scaffidi, C., Bretz, J.D., Zhang, M., Gentz, R.*, et al.* (1996). FLICE, a novel FADD-homologous ICE/CED-3-like protease, is recruited to the CD95 (Fas/APO-1) death--inducing signaling complex. Cell *85*, 817-827.
O'Carroll, D., Erhardt, S., Pagani, M., Barton, S.C., Surani, M.A., and Jenuwein, T. (2001). The polycomb-group gene Ezh2 is required for early mouse development. Mol Cell Biol *21*, 4330-4336.
Ozdogan, S., Kafadar, A., Yilmaz, S.G., Timirci-Kahraman, O., Gormus, U., and Isbir, T. (2017). Role of Caspase-9 Gene Ex5+32 G>A (rs1052576) Variant in Susceptibility to Primary Brain Tumors. Anticancer Res *37*, 4997-5000.
Pasini, D., Bracken, A.P., Hansen, J.B., Capillo, M., and Helin, K. (2007). The polycomb group protein Suz12 is required for embryonic stem cell differentiation. Mol Cell Biol *27*, 3769-3779.
Pasini, D., Bracken, A.P., Jensen, M.R., Lazzerini Denchi, E., and Helin, K. (2004). Suz12 is essential for mouse development and for EZH2 histone methyltransferase activity. EMBO J *23*, 4061-4071.
Pereira, J.D., Sansom, S.N., Smith, J., Dobenecker, M.W., Tarakhovsky, A., and Livesey, F.J. (2010). Ezh2, the histone methyltransferase of PRC2, regulates the balance between self-renewal and differentiation in the cerebral cortex. Proc Natl Acad Sci U S A *107*, 15957-15962.
Perkins, N.D., Felzien, L.K., Betts, J.C., Leung, K., Beach, D.H., and Nabel, G.J. (1997). Regulation of NF-kappaB by cyclin-dependent kinases associated with the p300 coactivator. Science *275*, 523-527.
Pouponnot, C., Jayaraman, L., and Massague, J. (1998). Physical and functional interaction of SMADs and p300/CBP. J Biol Chem *273*, 22865-22868.
Puffenberger, E.G., Jinks, R.N., Sougnez, C., Cibulskis, K., Willert, R.A., Achilly, N.P., Cassidy, R.P., Fiorentini, C.J., Heiken, K.F., Lawrence, J.J.*, et al.* (2012). Genetic mapping and exome sequencing identify variants associated with five novel diseases. PLoS One *7*, e28936.
Ramirez, F., Dundar, F., Diehl, S., Gruning, B.A., and Manke, T. (2014). deepTools: a flexible platform for exploring deep-sequencing data. Nucleic Acids Res *42*, W187-191.
Renier, N., Wu, Z., Simon, D.J., Yang, J., Ariel, P., and Tessier-Lavigne, M. (2014). iDISCO: a simple, rapid method to immunolabel large tissue samples for volume imaging. Cell *159*, 896-910.
Robinson, M.D., and Oshlack, A. (2010). A scaling normalization method for differential expression analysis of RNA-seq data. Genome Biol *11*, R25.
Rodriguez, C.I., Buchholz, F., Galloway, J., Sequerra, R., Kasper, J., Ayala, R., Stewart, A.F., and Dymecki, S.M. (2000). High-efficiency deleter mice show that FLPe is an alternative to Cre-loxP. Nat Genet *25*, 139-140.
Ronellenfitsch, M.W., Oh, J.E., Satomi, K., Sumi, K., Harter, P.N., Steinbach, J.P., Felsberg, J., Capper, D., Voegele, C., Durand, G.*, et al.* (2018). CASP9 germline mutation in a family with multiple brain tumors. Brain Pathol *28*, 94-102.
Sclafani, A.M., Skidmore, J.M., Ramaprakash, H., Trumpp, A., Gage, P.J., and Martin, D.M. (2006). Nestin-Cre mediated deletion of Pitx2 in the mouse. Genesis *44*, 336-344.
Skene, P.J., and Henikoff, S. (2017). An efficient targeted nuclease strategy for high-resolution mapping of DNA binding sites. Elife *6*.
Smolewski, P., Bedner, E., Du, L., Hsieh, T.C., Wu, J.M., Phelps, D.J., and Darzynkiewicz, Z. (2001). Detection of caspases activation by fluorochrome-labeled inhibitors: Multiparameter analysis by laser scanning cytometry. Cytometry *44*, 73-82.
Sommer, L., and Rao, M. (2002). Neural stem cells and regulation of cell number. Prog Neurobiol *66*, 1-18.
Spellicy, C.J., Norris, J., Bend, R., Bupp, C., Mester, P., Reynolds, T., Dean, J., Peng, Y., Alexov, E., Schwartz, C.E.*, et al.* (2018). Key apoptotic genes APAF1 and CASP9 implicated in recurrent folate-resistant neural tube defects. Eur J Hum Genet *26*, 420-427.
Srinivasula, S.M., Ahmad, M., Fernandes-Alnemri, T., and Alnemri, E.S. (1998). Autoactivation of procaspase-9 by Apaf-1-mediated oligomerization. Mol Cell *1*, 949-957.

Subramanian, A., Tamayo, P., Mootha, V.K., Mukherjee, S., Ebert, B.L., Gillette, M.A., Paulovich, A., Pomeroy, S.L., Golub, T.R., Lander, E.S.*, et al.* (2005). Gene set enrichment analysis: a knowledge-based approach for interpreting genome-wide expression profiles. Proc Natl Acad Sci U S A *102*, 15545-15550.
Takeuchi, T., Yamazaki, Y., Katoh-Fukui, Y., Tsuchiya, R., Kondo, S., Motoyama, J., and Higashinakagawa, T. (1995). Gene trap capture of a novel mouse gene, jumonji, required for neural tube formation. Genes Dev *9*, 1211-1222.
Thomaidou, D., Mione, M.C., Cavanagh, J.F., and Parnavelas, J.G. (1997). Apoptosis and its relation to the cell cycle in the developing cerebral cortex. J Neurosci *17*, 1075-1085.
Topper, J.N., DiChiara, M.R., Brown, J.D., Williams, A.J., Falb, D., Collins, T., and Gimbrone, M.A., Jr. (1998). CREB binding protein is a required coactivator for Smad-dependent, transforming growth factor beta transcriptional responses in endothelial cells. Proc Natl Acad Sci U S A *95*, 9506-9511.
Tronche, F., Kellendonk, C., Kretz, O., Gass, P., Anlag, K., Orban, P.C., Bock, R., Klein, R., and Schutz, G. (1999). Disruption of the glucocorticoid receptor gene in the nervous system results in reduced anxiety. Nat Genet *23*, 99-103.
Vanden Berghe, W., De Bosscher, K., Boone, E., Plaisance, S., and Haegeman, G. (1999). The nuclear factor-kappaB engages CBP/p300 and histone acetyltransferase activity for transcriptional activation of the interleukin-6 gene promoter. J Biol Chem *274*, 32091-32098.
von Schimmelmann, M., Feinberg, P.A., Sullivan, J.M., Ku, S.M., Badimon, A., Duff, M.K., Wang, Z., Lachmann, A., Dewell, S., Ma'ayan, A.*, et al.* (2016). Polycomb repressive complex 2 (PRC2) silences genes responsible for neurodegeneration. Nat Neurosci *19*, 1321-1330.
Wang, F., Flanagan, J., Su, N., Wang, L.C., Bui, S., Nielson, A., Wu, X., Vo, H.T., Ma, X.J., and Luo, Y. (2012). RNAscope: a novel in situ RNA analysis platform for formalin-fixed, paraffin-embedded tissues. J Mol Diagn *14*, 22-29.
Xu, S., Grullon, S., Ge, K., and Peng, W. (2014). Spatial clustering for identification of ChIP-enriched regions (SICER) to map regions of histone methylation patterns in embryonic stem cells. Methods Mol Biol *1150*, 97-111.
Yang, X., Li, C., Herrera, P.L., and Deng, C.X. (2002). Generation of Smad4/Dpc4 conditional knockout mice. Genesis *32*, 80-81.
Yu, M., Riva, L., Xie, H., Schindler, Y., Moran, T.B., Cheng, Y., Yu, D., Hardison, R., Weiss, M.J., Orkin, S.H.*, et al.* (2009). Insights into GATA-1-mediated gene activation versus repression via genome-wide chromatin occupancy analysis. Mol Cell *36*, 682-695.
Zhong, H., Voll, R.E., and Ghosh, S. (1998). Phosphorylation of NF-kappa B p65 by PKA stimulates transcriptional activity by promoting a novel bivalent interaction with the coactivator CBP/p300. Mol Cell *1*, 661-671.
Zhou, X., Zeng, W., Li, H., Chen, H., Wei, G., Yang, X., Zhang, T., and Wang, H. (2018). Rare mutations in apoptosis related genes APAF1, CASP9, and CASP3 contribute to human neural tube defects. Cell Death Dis *9*, 43.